A Study on Robust Slip Suppression Control of Electric Vehicles

Graduate School of Systems and Information Engineering

University of Tsukuba

March 2015

Shaobo Li

Abstract

This study presents a robust control method for slip suppression of electric vehicles (EVs) during accelerating. This method focuses on improving the traveling performance and low energy consumption of EVs by suppressing the wheel slip on roads with various surface condition and a range of mass. In this study, the extended Sliding Mode Control (SMC) method introducing the integral term with gain, where the integral gain is designed based on Model Predictive Control (MPC) algorithm, is proposed to improve the control performance. The numerical simulation shows the effectiveness of the proposed method.

Contents

List of Figures

List of Tables

Chapter 1

Introduction

1.1 Background and Objective

Along with the economic development, automobiles have become popular all over the world. In particular, over the past 10 years, the automobile population has been increasing rapidly in the developing countries, such as BRICs (Brazil, Russia, India and China) [1, 2]. With the wide spread of automobiles all over the world, especially internal-combustion engine vehicles (ICEVs), the environment and energy problems: air pollution, global warming, oil resource exhaustion and so on, are going severely [3, 4].

As a countermeasure to these problems, the development of next-generation vehicles such as hybrid vehicles (HVs: e.g., Toyota Prius, Ford C-Max Hybird, Honda Grace Hybrid, Volkswagen Jetta Hybrid) and electric vehicles (EVs: e.g., Mitsubishi i-MiEV, Nissan Leaf, Honda Fit EV, Tesla Model S) have been focused. EVs run on electricity only and they are zero emission and eco-friendly. So EVs have attracted great interests as a powerful solution

against the problems mentioned above [5–7].

EVs are automobiles which are propelled by an electric motor (or motors), using electrical energy stored in batteries or another energy storage devices. Compared with (internal-combustion engines) ICEs, EVs have several advantages as follows [8]: (a) Environmentally friendly. EVs do not emit any tailpipe pollutants, although the power plant producing the electricity may emit them. Electricity from solar-powered, nuclear-powered, hydro-powered or wind-powered plants causes no air pollutants. (b) Energy efficient. EVs convert 59-62% of the electrical energy from the grid to power at the wheels, but conventional gasoline vehicles only convert 17-21% of the energy stored in gasoline to power at the wheels. (c) Performance benefits. Electric motors provide quiet, smooth operation and stronger acceleration and require less maintenance than ICEs. (d) Reduce energy dependence. Electricity is a domestic energy source, which is essential contributor to the countries's energy security.

Contrary to the advantages described above, EVs have faced significant battery-related challenges to be widespread in use, such as travel distance per charge, recharge time, battery cost and weight. However, researchers are working on solving these problems and have made some progress. The exciting thing is that several EVs have offered for sale to the public. In Japan, Mitsubishi i-MiEV was launched for fleet customers in July 2009, and on April 1, 2010, for the wider public. Nissan Leaf was delivered to individual customers from December 2010 in the United States and Japan market. Tesla Model S, a leader in the EV market now, began its production in June 2012. It has achieved rapidly growing sales, particularly in Norway and USA. The US EPA official range for Model S Performance model equipped with an 85 kWh battery pack is 460 km, which shows an excellent battery performance than

other EVs (the range is about 200-300 km) [9].

The travel distance on a single charge for EV has been increased through battery improvements and using regeneration brakes, and the attention has been focused on improving motor performance. The following facts are viewed as relatively easy ways to improve maneuverability and stability of EVs [10].

1) The input/output response is faster than for gasolinediesel engines. It is said that the motor torque response is 2 orders of magnitude faster than that of the engine. E.g., if engine torque response costs 500 ms, the response time of motor toque will be 5 ms.
2) The torque generated in the wheels can be detected relatively accurately. For engine, the output torque varies along with the temperature and revolutions, even it has high-nonlinearity. Consequently the value of torque is too difficult to be measured accurately. However, the value of motor torque is surveyed easily and accurately from the view of current control.
3) The motor can be made small enough, then the vehicles can be made smaller by using multiple motors placed closer to the wheels. The drive wheels can be controlled fully and independently. E.g., it becomes easily achievable to control the differences of driving force developed between the left and right wheel.

Over the past few decades, a considerable number of studies have been conducted on the stability of general automobiles, for example, ABS (Anti-lock Braking Systems) [11], TCS (Traction Control System) [12], and ESC (Electric Stability Control) [13] as well as VSC (Vehicle Stability Control) [14], VSA (Vehicle Stability Assist) [15] and AWC (All Wheel

Control) [16]. What all of these have in common is that they maintain a suitable tire grip margin and reduce drive force loss to stabilize the vehicle behavior and improve drive performance. With gasoline/diesel engines, however, the response time from accelerator input until the drive force is transmitted to the wheels is slow and it is difficult to accurately determine the drive torque, which limits the vehicle's control performance.

When the vehicle is starting off or accelerating on slippery road, the driving wheels fall into slip easily, this leads to unstable driving situation and considerable waste of energy. A TCS is required to ensure the most driving force for driving wheels when accelerating, especially in slippery road conditions. Conventional gasoline/diesel vehicles are equipped with a TCS, which requires expensive sensors and additional equipment, but, as mentioned above, EV have a fast torque response and the motor characteristics can be used to accurately determined the torque, which makes it relatively easy and inexpensive to realize high-performance traction control [17, 18]. This is expected to improve the maneuverability and stability of EV. It is, therefore, important to research and development to achieve high-performance EV traction control with slip suppression.

Various proposals have been made for EV traction control, such as a system based on motor torque current dropping characteristics [19], a system that utilizes a nonlinear controller [20], and a system that controls the slip ratio with wheel control [21]. This research deals with the slip suppression of EV for controlling the wheel slip ratio. For the traction control by using the slip ratio, there are several methods proposed, such as the method based on MFC (Model Following Control) [22] and MP-PID (Model Predictive PID) method in [23]. Both show good performances under the nominal conditions where the situations, for example,

mass of the vehicle, road condition, and so on, are not changed. On one hand, to meet the high performance even variation happened in these conditions, it is significant to construct the robust control systems against the changing of situation. On the other hand, SMC (Sliding Mode Control), as one of the advanced control strategies, has performed good robustness for the systems with uncertainties or nonlinearities [24]. Many robust control methods for traction control based on SMC have been proposed [25, 26]. About this point, we propose a slip ratio control method which is based on SMC.

For SMC, by designing a switching control law, the trajectories move towards the sliding surface designed, once the states hit the sliding surface, the system trajectories can not leave it. Consequently the dynamic uncertainties can be tolerated. In order to obtain a good performance, the design of the sliding surface is very important. For slip suppression with the conventional approaches designed the sliding surface chosen by a linear trajectory of tracking error [27]. However, the control performance will get degradation due to the chattering which always occurs when switching the control inputs due to the structure of SMC [28]. To overcome such disadvantages, the SMC method introducing the integral action with gain to the design of the sliding surface (SMC-I) has been proposed by us [29], where the integral gain is derived by trial and error. In order to achieve better control performance and save more energy for slip suppression of EVs with changing the mass of the vehicle and road condition, the optimal integral gain adjusted on-line is required.

Since the late 1970s, Model Predictive Control (MPC) has developed considerable in the field of process industries [30–33]. As an advanced control method, many works have been developed and widely received by the academic world and industry. One advantage of MPC

is the ability to explicitly consider the constraints relating to the process. A conventional MPC makes explicit use of a model of the process to obtain the control input by optimizing an objective function. It have to be implemented to make the optimum calculation repeatedly on-line, as a result, the amount of computation required is even higher. So it had been only used in the controlled object which was a chemical or other systems with slow operating characteristics [34]. With the improvements in computing power of computer, the MPC algorithm is making possible increasing application in mechatronics and other areas, such as robots [35], solar plant [36], PVC plants [37], servomotor [38], vehicles [39].

So the SMC-I method based on model predictive control algorithm (MP-SMC-I) is presented to adjust the integral gain of SMC-I on-line by solving the optimization problem. The improvement to the performance of slip suppression control is expected.

In this dissertation, we present a new robust control method for slip suppression of EVs during acceleration with variations in road surface condition and loading conditions. Furthermore, the accelerating performance and energy saving performance of the method are further discussed.

1.2 Organization of Dissertation

The whole dissertation is composed of six chapters except preface and postscript. In chapter 2, we describe the general concept of SMC and discuss the robustness of SMC. Chapter 3 discusses the slip suppression control problem. Chapter 4 presents an extended SMC with integral action method (SMC-I), which takes the development of a robust controller for the slip ratio of EVs based on the sliding mode control. Numerical simulations are performed

to verify the effectiveness of SMC-I. In chapter 5, SMC with integral action based on MPC algorithm (MP-SMC-I) is proposed to determine the parameter of SMC-I, and the simulation results show the effectiveness of the proposed method. Finally, in chapter 6, concluding remarks are presented for the research performed in this dissertation and suggestions are made for directions of future work.

Chapter 2

Sliding Mode Control

In this chapter, the general concept of Sliding Mode Control (SMC) is introduced. The first steps of SMC theory originated in the early 1950's initiated in Former Soviet Union and started as Variable Structure Control (VSC) in 1970's [24] [40]. From 1980's, with the improvement of computer performance, SMC is applied in many control fields such as high-precision motor control [41], automotive control [42] and robot attitude control [43]. Now SMC is considered as an effective nonlinear-robust control method and have been attracted more and more attention.

2.1 Concept of SMC

SMC is one of the VSC methods. It is also a nonlinear control method that alters the dynamics of a nonlinear system by application of a high-frequency switching control. SMC utilizes discontinuous feedback control laws to force the system trajectory to reach, and subsequently

to remain on a specified surface within the state space (it's so called sliding or switching surface). The system dynamic when confined to the sliding surface is described as an ideal sliding motion and represents the controlled system behavior.

Consider the single input nonlinear system [28]

$$x^{(n)} = f(\mathbf{x}) + b(\mathbf{x})u \tag{2.1}$$

where u is the control input and $\mathbf{x} = [x \quad \dot{x} \quad ... \quad x^{(n-1)}]^T$ is the state vector. In general, the function $f(\mathbf{x})$ and the control gain $b(\mathbf{x})$ are nonlinear. In Equation (2.1), $f(\mathbf{x})$ and $b(\mathbf{x})$ are not exactly known, but the extents of the imprecision on $f(\mathbf{x})$ and $b(\mathbf{x})$ are upper bounded by known continuous functions of $\mathbf{x}$. The control problem is to seek a control law that makes the state $\mathbf{x}$ to track the desired state $\mathbf{x}^* = [x^* \quad \dot{x}^* \quad ... \quad x^{*(n-1)}]^T$ in the presence of model imprecision on $f(\mathbf{x})$ and $b(\mathbf{x})$.

Let us define a time-varying surface $S(t)$ in the state space $\mathbf{R}^{(n)}$ by the equation $s(\mathbf{x}; t)$ defined as follow,

$$S(t) = \{x | s(\mathbf{x}; t) = 0\} \tag{2.2}$$

where $s(\mathbf{x}; t)$ is defined by

$$s(\mathbf{x}; t) = \left(\frac{d}{dt} + \alpha\right)^{n-1} \mathbf{x_e}, \ \alpha > 0 \tag{2.3}$$

where $\mathbf{x_e} = \mathbf{x} - \mathbf{x}^* = [x_e \quad \dot{x}_e \quad ... \quad {x_e}^{(n-1)}]^T$ is the error between the output state and the desired state. The problem of tracking $\mathbf{x} \equiv \mathbf{x}^*$ is equivalent to remain on the surface $S(t)$ for all $t > 0$. From Equation (2.3), $s \equiv 0$ presents a linear differential equation whose unique solution is $\mathbf{x_e} \equiv 0$. Thus, the problem of tracking the n-dimensional vector $\mathbf{x}^*$ can be

replaced by a 1st order stabilization problem in s. When $s(\mathbf{x};t)$ equals 0, that is to say, the system trajectories reach the surface which represents the tracking error is 0. Here, $S(t)$ is known as sliding surface. On this surface, the error will converge to 0 exponentially.

This implies that if there exists a control input $u(t)$ such that $x(t)$ is in $S(t)$ and it satisfies that $x(\tau)$ is in $S(\tau)$ for all $\tau > t$, the error will converge exponentially to 0 for this control input.

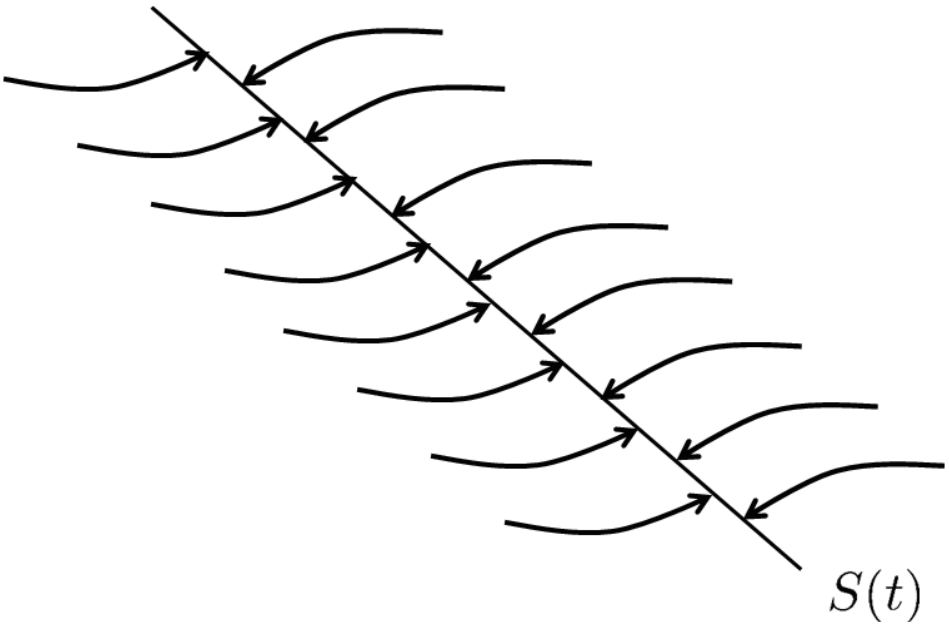

Figure 2.1 Graphical interpretation of the sliding condition

2.2 Robustness of SMC

The simplified 1st order problem of keeping the scalar s at 0 can now be achieved by choosing the control law u of Equation (2.1) such that outside of $S(t)$

$$\frac{1}{2}\frac{d}{dt}s^2 \leq -\eta|s| \tag{2.4}$$

where η is a strictly positive constant. Equation (2.4) is called sliding condition. From Equation (2.4) , s^2 shows that the squared distance to the sliding surface, which decreases along all system trajectories. As drawn in Figure 2.1, it implies trajectories to point towards the surface $S(t)$. Particularly, once the trajectories reach the surface, they also continue to be on the surface. That is to say, satisfying the sliding condition makes the trajectories reach the surface in finite time, and once on the manifold, they cannot leave off it. Furthermore, Equation (2.4) also implies that some disturbances or dynamic uncertainties can be tolerated while still keeping the surface an invariant set.

Meeting Equation (2.3) makes that if $x(t=0)$ is off $x^*(t=0)$, the surface $S(t)$ will be reached in a finite time smaller than $|s(t=0)|/\eta$. Assume for instance that $s(t=0)>0$, t_r is defined as the time requited to hit the surface $s=0$. Below is the deduction process of t_r. First, for $s(t)>0$ in $t>0$, Equation (2.4) can be rewritten as

$$\dot{s} \leq -\eta. \tag{2.5}$$

Integrating Equation (2.5) between $t=0$ and t_r leads to

$$\begin{aligned} \int_0^{t_r} \dot{s}dt &= s(t=t_r) - s(t=0) \\ &= 0 - s(t=0) \leq -\eta(t_r - 0) \end{aligned} \tag{2.6}$$

which implies that

$$t_r \leq s(t=0)/\eta. \tag{2.7}$$

The similar result starting with $s(t=0)<0$, can be obtained, and thus

$$t_r \leq |s(t=0)|/\eta. \tag{2.8}$$

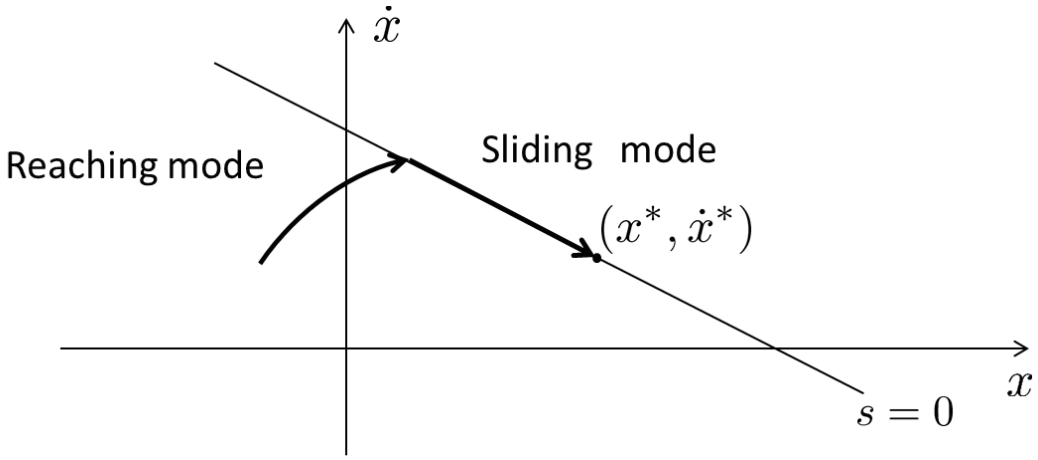

Figure 2.2 The behavior of system trajectory in SMC ($n = 2$)

Figure 2.2 is the graphical interpretation of Equations (2.3) and (2.4) when $n = 2$. It shows there are two modes in SMC, which are the reaching mode and the sliding mode. From this figure, the state trajectory starting from any initial condition, reaches the sliding surface in a finite time smaller than $|s(t = 0)|/\eta$ (in the reaching mode), and then slides along the surface towards $\mathbf{x}^*(t)$ exponentially (in the sliding mode). In next section, the two modes will be achieved by deriving the control input.

2.3 Implementation of SMC

In general, to design a control system based on SMC should go through the following two steps:

- Design a sliding surface that is invariant of the controlled dynamics.
- Define the control input that drives the system trajectory to the sliding surface in sliding mode in finite time.

In this section, we will discuss these two steps. Considering the system equation (2.1) defined in the previous section, assume that for all x, $b(\mathbf{x}) \neq 0$. We derive a control such that $\dot{s} = 0$ when the sliding mode exists, Equation (2.3) can be rewrite as

$$s = x_e^{(n-1)} + ... + \alpha^{n-1} x_e. \tag{2.9}$$

Differentiate Equation (2.9), we can obtain that

$$\begin{aligned} \dot{s} &= x_e^{(n)} + ... + \alpha^{n-1}\dot{x}_e \\ &= x^{(n)} - x^{*(n)} + ... + \alpha^{n-1}\dot{x}_e \\ &= f(\mathbf{x}) + b(\mathbf{x})u - x^{*(n)} + ... + \alpha^{n-1}\dot{x}_e \end{aligned} \tag{2.10}$$

while the dynamics is in sliding mode,

$$\dot{s} = 0. \tag{2.11}$$

By solving the equation for the control input, $u = u_{eq}$,

$$u_{eq} = \frac{1}{b(\mathbf{x})}\big(-f(\mathbf{x}) + x^{*(n)} - ... - \alpha^{n-1}\dot{x}_e\big). \tag{2.12}$$

Here, u_{eq} is called the equivalent control input, which can be interpreted as the control law that would maintain $\dot{s} = 0$ if the dynamics were in the sliding mode. However, if the system trajectory is not on the sliding surface (the reaching mode), an another item has to be added to the control input to drive the system to the sliding surface. In the reaching mode, the switching control u_{sw} makes the trajectory from the initial trajectory to the sliding surface and it can be defined as

$$u_{sw} = -\frac{K}{b(\mathbf{x})}\text{sgn}(s) \tag{2.13}$$

where

$$\text{sgn}(s) = \begin{cases} -1, & s < 0 \\ 0, & s = 0 \\ 1, & s > 0 \end{cases} \tag{2.14}$$

and K is called sliding gain.

In Equation (2.13), the switching control using the discontinuous function requires infinitely fast switching, but in real systems, the sampling and delays in digital implementation causes s to pass to the other side of the surface $S(t)$, which produces chattering. Chattering is high-frequency finite oscillations which is caused by switching of the variable s around the sliding surface $S(t)$. A solution to reduce chattering introduces a region around $S(t)$ called boundary layer so that s changes its value continuously [28]. Normally, a smooth continuous switching, sat$(\frac{s}{\Phi})$ is chosen to replace the discontinuous switching, sgn(s). The function sat$(\frac{s}{\Phi})$ is defined as

$$\text{sat}\left(\frac{s}{\Phi}\right) = \begin{cases} -1, & s < -\Phi \\ \dfrac{s}{\Phi}, & -\Phi \leq s \leq \Phi \\ 1, & s > \Phi \end{cases} \tag{2.15}$$

where $\Phi > 0$ is a design parameter representing the width of the boundary layer around the sliding surface $s = 0$. With this replacement, the sliding surface function s with an arbitrary

initial value will reach and stay within the boundary layer $|s| \leq \Phi$. Figure 2.3 illustrates the sign function and the saturation function. From Equation (2.13), the switching control is

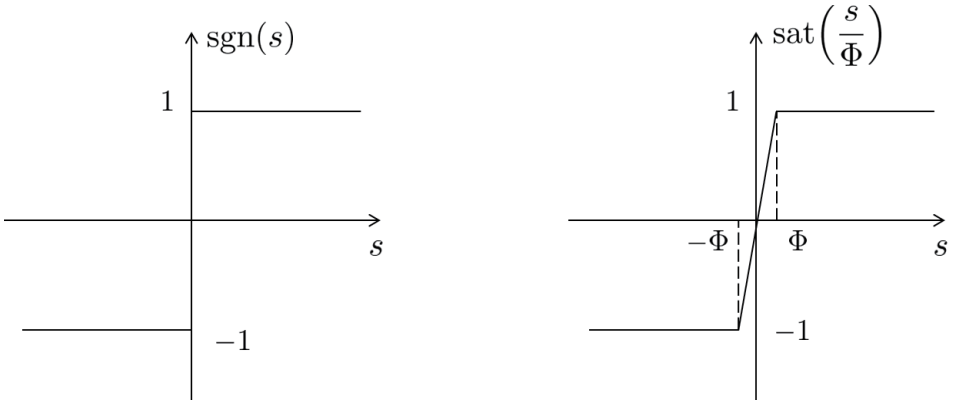

Figure 2.3 Sign function and saturation function

rewritten by using sat$(\frac{s}{\Phi})$ as

$$u_{sw} = -\frac{K}{b(\mathbf{x})}\text{sat}\Big(\frac{s}{\Phi}\Big). \tag{2.16}$$

Finally, the SMC control law can be defined as

$$\begin{aligned} u &= u_{eq} + u_{sw} \\ &= \frac{1}{b(\mathbf{x})}\Big(-f(\mathbf{x}) + x^{*(n)} - ... - \alpha^{n-1}\dot{x}_e - K\text{sat}\Big(\frac{s}{\Phi}\Big)\Big). \end{aligned} \tag{2.17}$$

In summary, when the trajectory is on the sliding surface ($s = 0$), it is desired to have $u_{sw} = 0$, the switching control has no effect on the sliding surface. Moreover, when the trajectory is off the sliding surface or the uncertainty in the system occurs, the switching control acts to return the trajectory back to the sliding surface. Therefore, the total control u causes the system to keep the trajectory on the sliding surface.

Chapter 3

Slip Suppression Control Problem

3.1 Electric Vehicles with In-wheel Motors

EVs, green vehicles, are propelled by an electric motor (or motors) powered by rechargeable battery packs. They produce zero emissions at the point of use. An electric motor is 400% to 600% more efficient than an ICE. EVs can use electricity from anywhere including sustainable energy resources (e.g., hydro power, wind and sun). Besides, EVs are simple, silent, and affordable to operate.

For EVs, one of the more interesting designs, the motor-wheel assembly is an elegant integration of electric motor and other components into a package that fits inside a regular-size tire, which is called in-wheel motor. In fact, the car equipped with in-wheel motors was developed in the end of the 19th century. The growth in power of the gasoline engine was so fast that it eventually overtook the power of the electric in-wheel motors, even though any losses was made up through a transmission. As a result the car moved to gas engines with

transmissions, but they were never as efficient as electric in-wheel motor. Since the late 20th century, owing to the development of battery technology and enhancement of environmental awareness, in-wheel motors have again been used on cars.

In-wheel motors do not require gearboxes, drive shafts or differentials thus giving far greater flexibility to vehicle designer while substantially reducing drive train losses. The reduced drive train losses mean less energy is wasted (during both acceleration and regenerative braking), resulting in more of the energy from the battery pack being available to propel the vehicle. Especially, each in-wheel motor can be controlled entirely independently, providing far greater control, performance and vehicle dynamics than any other drive system. In addition, traction control, launch control and torque vectoring are all easily implemented through the use of in-wheel motors. Therefore, they have received much attention to be applied to the next-generation EVs. In this research, we proposed the wheel slip control method for EVs with in-wheel motors.

3.2 Vehicle Dynamics

Vehicle model which is appropriate for acceleration limited to the longitudinal direction, is descried. As mentioned above, in-wheel motors can be attached independently in four wheels and easily steered and controlled, so one wheel car model is used as the control object, which can be also extended to all wheels control. Although the one wheel car model is quite simple, it keeps the essential dynamics of the system. The one wheel car model shown in Figure 3.1 is considered in this study. This model only includes longitudinal motion with one driving force input. For simplicity's sake, the rolling resistance of the wheel and air resistance of the

vehicle are both ignored.

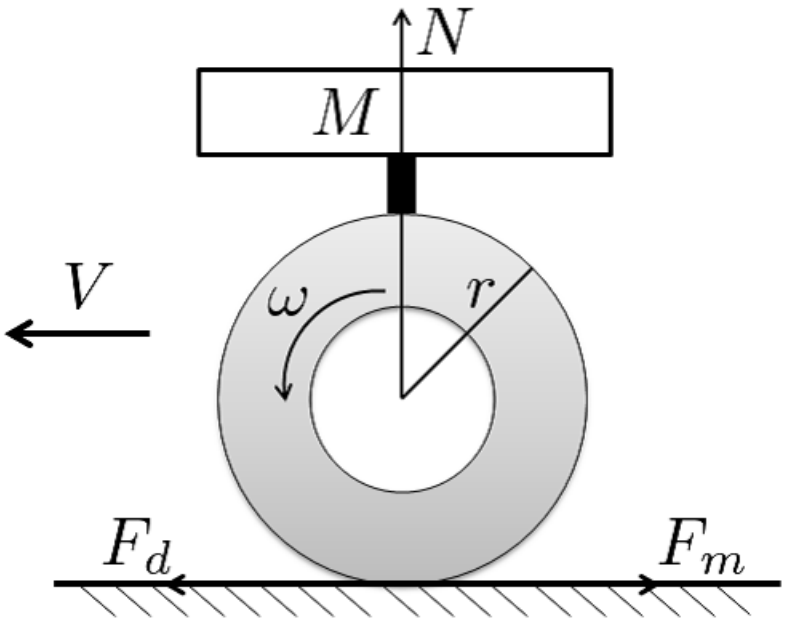

Figure 3.1 One wheel model of cars

The driving force and wheel friction are in the direction of motion. The wheel is rotating in an anticlockwise direction, and slipping against the ground. This slipping generates the driving force toward left causing the vehicle to accelerate. The wheel directly driven by an electrical motor is used for system analysis, design of control laws and numerical simulations.

The dynamic equation for the wheel rotating motion is

$$J_w\dot{\omega} = T_m - rF_d \tag{3.1}$$

and the dynamic equation for the vehicle motion is given as

$$M\dot{V} = F_d. \tag{3.2}$$

All the parameters in both equations are defined in Table 3.1.

Table 3.1 Vehicle model parameters

J_w	Inertia of the wheel
ω	Angular velocity of the wheel
T_m	Driving toque
r	Radius of the wheel
F_d	Driving force
M	Mass of the vehicle
V	Vehicle body velocity

F_m is the force equivalent value of the driving toque, and it is defined as

$$F_m = \frac{T_m}{r}. \tag{3.3}$$

A driving torque applied to a tire generates a driving force at the tire-road contact patch which is equal to the viscous friction force of the wheel. The friction force developed on the tire-road contact surface depends on the wheel slip, which is defined behind. The tire driving force F_d is given by

$$F_d = \mu(c, \lambda)N \tag{3.4}$$

where $\mu(c, \lambda)$ is the friction coefficient as hereinafter defined and the normal tire force N is defined as

$$N = Mg \tag{3.5}$$

where g is the acceleration of gravity.

3.3 Slip Suppression Control Problem Based on Slip Ratio

The friction coefficient $\mu(c, \lambda)$, which is the ratio between the driving force and the normal tire force, depends on the road condition (represented by road condition coefficient c) and the wheel slip (represented by the slip ratio λ). The slip ratio of the wheel is defined as the difference between the wheel and body velocities, divided by the maximum of these velocity values (wheel velocity for acceleration, vehicle body velocity for braking), and given by

$$\lambda = \begin{cases} \dfrac{V_\omega - V}{V_\omega} & \text{(accelerating)} \\ \\ \dfrac{V - V_\omega}{V} & \text{(braking)} \end{cases} \tag{3.6}$$

where $V_\omega = r\omega$ is the wheel velocity. λ during accelerating can be shown by Equation (3.7) from Figure 3.1,

$$\lambda = \frac{r\omega - V}{r\omega}. \tag{3.7}$$

The value of $\lambda = 0$ characterizes the free motion of the wheel where no wheel slip happens (no friction force is exerted). If the slip attains the value $\lambda = 1$, then the wheel is completely skidding. The friction forces that are generated between the road surface and the tires are the force generated in the longitudinal direction of the tires and the lateral force acting perpendicularly to the vehicle direction of travel, and both of these are expressed as a function of λ. The friction force generated in the tire longitudinal direction is expressed as μ, and the relationship between μ and λ is shown by Equation (3.8) below, which is a formula called

the **Magic-Formula** and gives values compatible with experimental data given in [44]. It is simplified and has been using in earlier study in [22].

$$\mu(c,\lambda) = -c \times 1.1 \times \left(e^{-35\lambda} - e^{-0.35\lambda}\right) \tag{3.8}$$

where c is the coefficient used to determine the road condition and was found by experimental data to be approximately $c = 0.8$ for general dry asphalt roads, approximately $c = 0.5$ for general wet asphalt roads, and approximately $c = 0.12$ for icy road. In the simulations, this formula is used for estimating the maximum value of friction coefficient. For the various road conditions ($0 < c < 1$), the $\mu(c,\lambda)$ surface is shown in Figure 3.2.

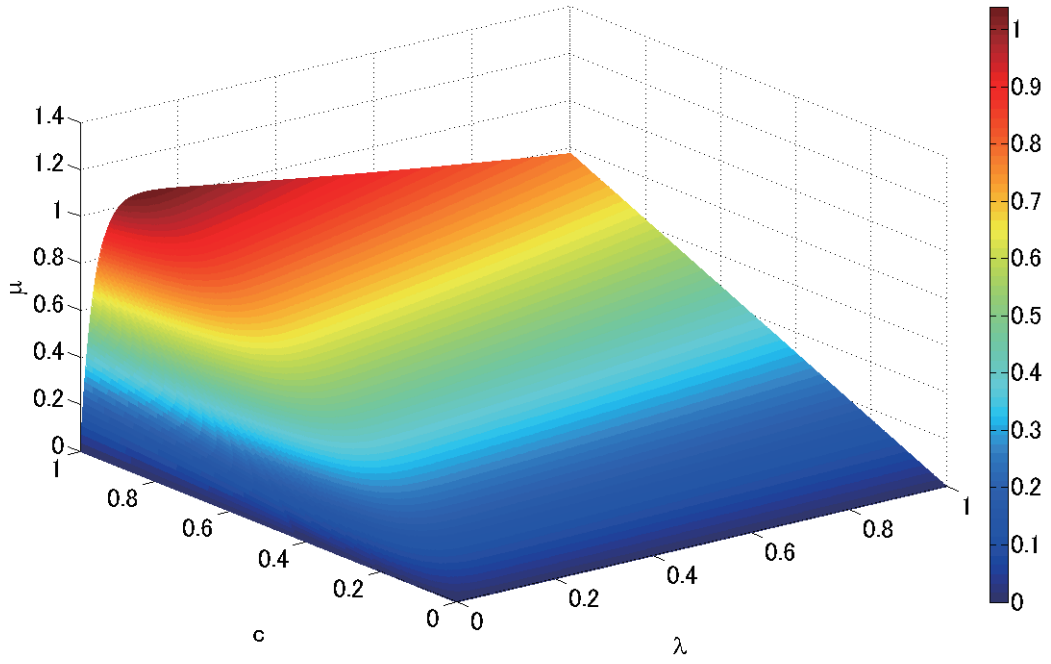

Figure 3.2 $\mu - \lambda$ surface for road conditions

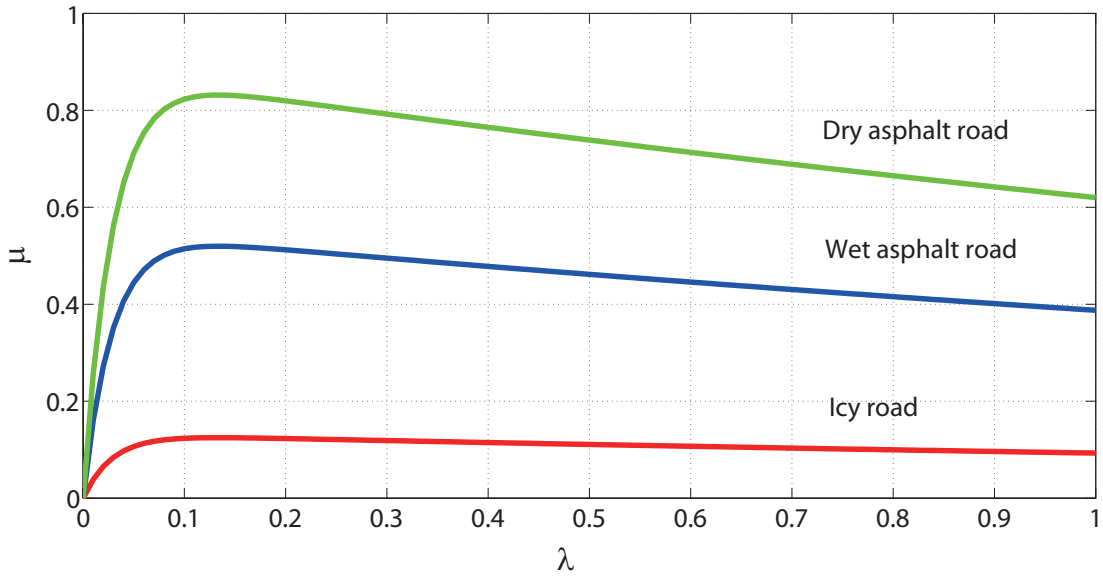

Figure 3.3 $\mu - \lambda$ curve

3.3.1 Reference Value of Slip Ratio

The $\mu - \lambda$ curve for acceleration case is shown in Figure 3.3 on three different road conditions (dry asphalt, wet asphalt and icy road). It shows how the friction coefficient μ increases with slip ratio λ up to a value λ^* ($0.1 < \lambda^* < 0.2$) where it attains the maximum value of the friction coefficient. As defined in (3.4), the driving force also achieves the maximum value in corresponding to the friction coefficient. However, the friction coefficient decreases to the minimum value when the wheel is completely skidding. Therefore, to achieve the maximum value of driving force for slip suppression, λ should be maintained at the desired value λ^*. The value of λ^* is derived as follows.

Choose the function $\mu_c(\lambda)$ defined as

$$\mu_c(\lambda) = -1.1 \times \left(e^{-35\lambda} - e^{-0.35\lambda}\right). \tag{3.9}$$

By using Equation (3.9), Equation (3.8) can be rewritten as

$$\mu(c, \lambda) = c \cdot \mu_c(\lambda). \tag{3.10}$$

Evaluating the values of λ which maximize $\mu(c, \lambda)$ for different $c(c > 0)$, means to seek the value of λ where the maximum value of the function $\mu_c(\lambda)$ can be obtained. Then let

$$\frac{d}{d\lambda}\mu_c(\lambda) = 0 \tag{3.11}$$

and solving Equation (3.11) gives

$$\lambda = \frac{log100}{35 - 0.35} \tag{3.12}$$

$$\approx 0.13. \tag{3.13}$$

Therefore, for the different road conditions, when $\lambda \approx 0.13$ is satisfied, the maximum driving force can be gained. Namely, from Equation (3.8) combined with Figures 3.2 and 3.3 we find that regardless of the road condition (value of c), the $\mu - \lambda$ surface attains the largest value of μ when λ is the optimal value 0.13. So in this dissertation, desired value of slip ratio is set by $\lambda^* = 0.13$.

3.3.2 Problem Formulation

To attain the maximum driving force, λ is needed to maintain at λ^* stably and accurately in any case. However, in fact, the road surface on which vehicles travel is not always remain

unchangeable. Moreover, the vehicle mass varies when the weight of a load such as the luggage and passengers changes. Therefore, we need to control the slip ratio under the condition of the often change of road condition c and vehicle mass M. For this reason, a robust slip suppression control is needed.

The slip suppression problem is to construct a robust controller such that λ converges to 0.13 with parameter uncertainties in vehicle mass and road condition. The block diagram of the robust slip suppression control system is shown in Figure 3.4. As a robust controller, the SMC with integral action method is presented in the next Chapter.

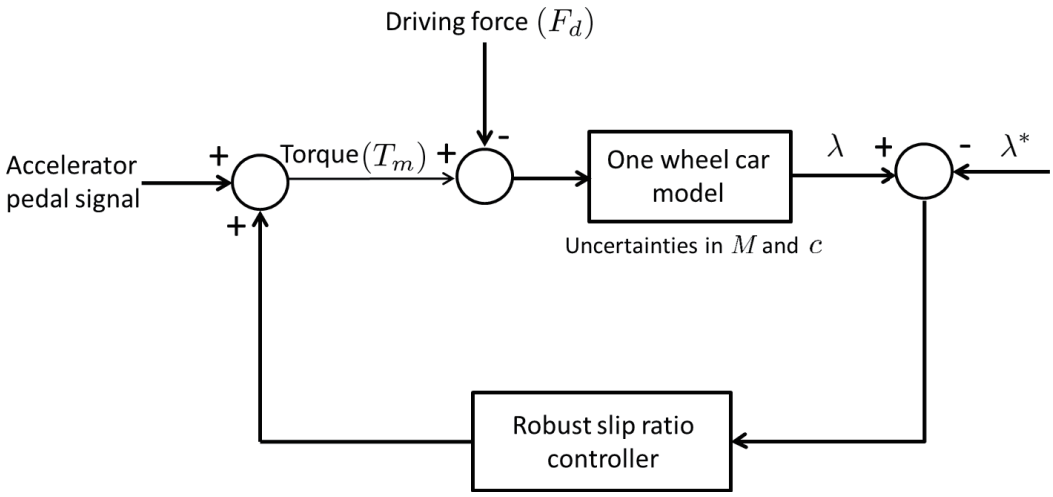

Figure 3.4 Block diagram of robust slip suppression control system

Chapter 4

SMC with Integral Action

4.1 Introduction

In SMC, the motion of the system trajectory can be divided into two modes. At first, the system trajectory is forced to reach a desired geometrical locus called sliding surface, which is reaching mode. Then the trajectory slides along this surface and converges to the desired value, when the motion of the system is in sliding mode. The system meeting the sliding condition makes the trajectories reach the surface in finite time, and once they are on the surface, they cannot leave it. This shows that some dynamic uncertainties can be tolerated by keeping the motion of the system in sliding mode. Hence, the control input of SMC consists of two parts: the hitting input taking the system trajectory to reach the sliding surface in finite time and the equivalent input keeping the system trajectory remains in the sliding surface.

In original SMC, chattering phenomenon always occurs through high frequently switching of the control input because of the variable structure of the sliding mode controller. To reduce

such undesired chattering effect, normally one boundary layer around the sliding surface is introduced by using a continuous control input. In contrast, the control performance such as steady state accuracy and transient response performance gets degradation.

According to [27], a robust slip suppression controller using conventional SMC method is presented to the anti-lock braking system (ABS). It improves the robustness of the system to the change of road conditions, but the control precision and energy evaluation are not discussed. To overcome these disadvantages of conventional SMC method applied to slip suppression of EVs, an improved method is required.

4.2 SMC with Integral Action Method

In this section, for slip suppression of EVs, the proposed control strategy based on SMC with integral action (SMC-I) is explained. Without loss of generality, one wheel car model described in chapter 3 is used for the design of the control law. The nonlinear system dynamics can be presented by a differential equation as

$$\dot{\lambda} = f + bT_m \tag{4.1}$$

where $\lambda \in R$ is the state of the system representing the slip ratio of the driving wheel which is defined as Equation (4.2) from Equation (3.6) for the case of acceleration, $T_m \in R$ is the control input representing the torque of the motor. So this is a SISO (Single Input and Single Output) system. f describes the nonlinearity of the system, b is the input gain, and they are all time-varying.

$$\lambda = \frac{V_\omega - V}{V_\omega}. \tag{4.2}$$

Differentiating Equation (4.2) with respect to time gives

$$\dot{\lambda} = \frac{-\dot{V} + (1-\lambda)\dot{V}_w}{V_w} \tag{4.3}$$

and substituting Equations (3.1), (3.2) and (3.4) in chapter 3 into Equation (4.3), the system dynamics can be rewritten as

$$\dot{\lambda} = -\frac{g}{V_w}\left[1 + (1-\lambda)\frac{r^2 M}{J_w}\right]\mu(c,\lambda) + \frac{(1-\lambda)r}{J_w V_w}T_m. \tag{4.4}$$

By reference to the system dynamics, the following equations can be attained,

$$f = -\frac{g}{V_w}\left[1 + (1-\lambda)\frac{r^2 M}{J_w}\right]\mu(c,\lambda) \tag{4.5}$$

$$b = \frac{(1-\lambda)r}{J_w V_w}. \tag{4.6}$$

4.2.1 Parameter Uncertainties in System Dynamics

The control objective is to control the value of the slip ratio λ to the constant reference λ^*. Actually, the mass of the car often changes with the number of passengers and the weight of luggage. Besides, the car has to always travel on various road surfaces. As a result, the controller needs to perform much robustly with the uncertainties happened in the mass of vehicle and road surface conditions which are represented by the viscous friction coefficient c and the vehicle mass M respectively. The ranges of variation in parameter c and parameter M are defined as

$$c_{min} \leq c \leq c_{max} \tag{4.7}$$

$$M_{min} \leq M \leq M_{max}. \tag{4.8}$$

Consider the system represented by Equation (4.1), the nonlinear function f is not exactly known, but estimated as f_n. The estimated error on f is assumed to be bounded by some known function $F = F(\lambda)$,

$$|f - f_n| \leq F. \tag{4.9}$$

The uncertainty in f is due to the parameter M and c, therefore, by using Equation (4.5), f_n can be defined as

$$f_n = -\frac{g}{V_w}\left[1 + (1-\lambda)\frac{r^2 M_n}{J_w}\right]\mu(c_n, \lambda) \tag{4.10}$$

where M_n is the estimated value of vehicle mass M and c_n is estimated for the viscous friction coefficient c.

Here, we define the estimated values of these parameters respectively as the arithmetic mean of the value of the bounds.

$$c_n = \frac{c_{min} + c_{max}}{2} \tag{4.11}$$

$$M_n = \frac{M_{min} + M_{max}}{2}. \tag{4.12}$$

From these definitions, the error in estimation is given by

$$f - f_n = -\frac{g}{V_w}\Big\{\big[\mu(c, \lambda) - \mu(c_n, \lambda)\big] + (1-\lambda)\frac{r^2}{J_w}\big[M\mu(c, \lambda) - M_n\mu(c_n, \lambda)\big]\Big\}. \tag{4.13}$$

Taking the absolute value of both sides of Equation (4.13), that can be obtained as

$$\begin{aligned} |f - f_n| \leq \frac{g}{|V_w|}\Big\{&\big|\mu(c_{max}, \lambda) - \mu(c_n, \lambda)\big| \\ &+ (1-\lambda)\frac{r^2}{J_w}\big|M_{max}\mu(c_{max}, \lambda) - M_n\mu(c_n, \lambda)\big|\Big\}. \end{aligned} \tag{4.14}$$

Then, let

$$F = \frac{g}{|V_w|}\Big\{\big|\mu(c_{max},\lambda) - \mu(c_n,\lambda)\big| + (1-\lambda)\frac{r^2}{J_w}\big|M_{max}\mu(c_{max},\lambda) - M_n\mu(c_n,\lambda)\big|\Big\}. \tag{4.15}$$

4.2.2 Design of Sliding Surface

As described in chapter 2, chattering always occurs in sliding mode design owing to the switching occurring on the sliding surface. In order to reduce this undesired chattering effect for which it is possible to excite the high frequency modes, normally one boundary layer around the sliding surface is introduced [28]. To eliminate chattering of the control input signal, larger width of the boundary layer is required. However, for better tracking accuracy, a boundary layer with a smaller width is preferred.

By using the conventional SMC method, because the order of the system is assumed to be one, the sliding function can be given by

$$s_c(\lambda,t) = \lambda_e \tag{4.16}$$

where λ_e is the error between the actual slip ratio and the desired value, which is represented as $\lambda_e = \lambda - \lambda^*$. In order to improve the transient performance of the control system and the steady-state accuracy of response of slip ratio using the conventional SMC method, an integral action is added to the sliding function $s_c(\lambda,t)$. The new sliding function s can be

rewritten as

$$\begin{aligned} s(\lambda, t) &= \lambda_e + K_{in} \int_0^t \lambda_e(\tau) d\tau \\ &= (\lambda - \lambda^*) + K_{in} \int_0^t \big[(\lambda(\tau) - \lambda^*(\tau)\big] d\tau \end{aligned} \tag{4.17}$$

where K_{in} is the integral gain, $K_{in} \geq 0$. When $K_{in} = 0$, the new sliding function becomes the same as the conventional one.

4.2.3 Derivation of Control Law

In this section, the sliding mode controller is derived to make the slip ratio λ to converge the desired value λ^*. The sliding mode happens when the system trajectory reaches the sliding surface defined by $s = 0$. The dynamics of sliding mode are governed by

$$\dot{s} = 0. \tag{4.18}$$

Differentiating Equation (4.17), then substituting the result into Equation (4.18) gives

$$(\dot{\lambda} - \dot{\lambda}^*) + K_{in}(\lambda - \lambda^*) = 0. \tag{4.19}$$

In our research, the reference slip ratio λ^* is a constant, thus $\dot{\lambda}^* = 0$. Substituting Equation (4.1) into Equation (4.19) gives

$$f + bT_m + K_{in}(\lambda - \lambda^*) = 0 \tag{4.20}$$

and solving Equation (4.20) gives the equivalent control input as

$$T_{meq} = \frac{1}{b}\big[-f - K_{in}(\lambda - \lambda^*)\big] \tag{4.21}$$

then the estimate of the equivalent control can be obtained as

$$T_{meqn} = \frac{1}{b}\big[-f_n - K_{in}(\lambda - \lambda^*)\big]. \tag{4.22}$$

The equivalent control input T_{meqn} is used to maintain sliding in sliding mode. When the system trajectory is not on the sliding surface, the switching control input T_{msw} has to be added to drive the trajectory back to the sliding surface, which is defined by

$$T_{msw} = \frac{1}{b}\big[-K\text{sgn}(s)\big]. \tag{4.23}$$

where $K > 0$ is the sliding gain and sgn(s) is the sign function. Thus, the control law can be given by the sum of T_{meqn} and T_{msw} as

$$\begin{aligned} T_m &= T_{meqn} + T_{msw} \\ &= \frac{1}{b}\big[f_n - K_{in}(\lambda - \lambda^*) - K\text{sgn}(s)\big]. \end{aligned} \tag{4.24}$$

When there is no uncertainty existing in the system (i.e., no variation in c and M), T_{msw} is desired to be 0. Because Equation (4.24) contains the estimate of the equivalent control T_{meqn}, T_m keeps the trajectory on the sliding surface ($s = 0$ i.e., $\lambda = \lambda^*$). By reason of the uncertainties, the trajectory deviates from the sliding surface. The switching control acts to pull the trajectory back to the sliding surface which implies the robustness of SMC.

Here, the sliding gain K is selected by defining a Lyapunov candidate function that guarantees meeting the sliding condition

$$s\dot{s} \leq -\eta|s| \tag{4.25}$$

where $\eta > 0$ is a design parameter. Let the Lyapunov candidate function be defined as

$$V_L = \frac{1}{2}s^2. \tag{4.26}$$

Taking the time derivative of Equation (4.26) gives

$$\begin{aligned}\dot{V}_L &= \frac{1}{2}\frac{d}{dt}s^2 \\ &= s\dot{s}.\end{aligned} \tag{4.27}$$

Substituting Equation (4.17) into Equation (4.27) yields

$$\begin{aligned}\dot{V}_L &= s\big[f - f_n - K\text{sgn}(s)\big] \\ &= s(f - f_n) - K|s| \\ &\leq F|s| - K|s|.\end{aligned} \tag{4.28}$$

The sliding condition can be achieved form Equation (4.28) if K is selected as $K = F + \eta$.

Thus, the control law can guarantee the reaching and sustaining of the sliding mode. Concretely, the stability of the system is guaranteed with an exponential convergence once the sliding surface is encountered, if the sliding condition is satisfied. So Equation (4.28) guarantees that the strategy can converge to the sliding surface in finite time if the error is not zero, that is to say, slip ratio can be controlled to the reference slip ratio in finite time whenever the uncertainty occurs in the system.

4.2.4 Chattering Reduction

The control law defined by Equation (4.24) using a discontinuous sign function leads to chattering in control input. In general, the inherent high-frequency chattering of the control input may limit the practical application of SMC-I. A practical approach to avoid chattering is to using the smooth switching to replace discontinuous switching by introducing a region

around the sliding surface. Here we further replace sgn(s) in Equation (4.24) by the saturation function sat$\left(\frac{s}{\Phi}\right)$, where $\Phi > 0$ is a design parameter representing the width of the boundary layer around the sliding surface. By using this replacement, the sliding function s with an arbitrary initial value will reach and stay within the boundary layer $|s| \leq \Phi$. Then the control law of SMC-I controller can be represented as

$$T_m = \frac{1}{b}\left[f_n - K_{in}(\lambda - \lambda^*) - K\text{sat}\left(\frac{s}{\Phi}\right)\right]. \tag{4.29}$$

4.3 Simulation Examples

This section shows the simulation examples to confirm the effectiveness of the SMC-I method for the slip suppression control in accelerating. The numerical simulations have been carried out using MATLAB/Simulink and results are presented and compared. The computer configuration and simulation environment are shown in Table 4.1.

Table 4.1 Simulation environment

OS	Windows 7 Professional 32bit
CPU	Intel(R) Core(TM)2 Quad CPU Q8400 2.66GHz
RAM	4.00GB
Software	MATLAB 7.12.0.635 (R2011a) Student Version

4.3.1 Simulation Setup

The one wheel model described in chapter 3 is used for the simulations examples. The vehicle parameter values are listed in Table 4.2.

Table 4.2 Values of vehicle parameters used in the simulations

J_w: Inertia of wheel	21.1[$\mathrm{kg \cdot m^2}$]
r: Radius of wheel	0.26[m]
λ^*: Reference slip ratio	0.13
g: Acceleration of gravity	9.81[$\mathrm{m/s^2}$]

The width of the boundary layer Φ defined in Equation (4.29) is placed at 1 and the design parameter η is set to 10. In Equation (4.29), the SMC-I control law can be calculated with the value of K_{in}, which impacts on the steady state accuracy of slip ratio in this system. Here, in order to confirm the effectiveness for the energy conservation performance of the SMC-I method, the value of K_{in} is chosen as 6, which is determined by trail and error.

When K_{in} equals 0, the SMC-I method becomes the conventional SMC method. The control law of the conventional SMC can be derived as

$$T_{mc} = \frac{1}{b}\left[-f_n - (F+\eta)\mathrm{sat}\left(\frac{s}{\Phi}\right)\right]. \tag{4.30}$$

Likewise, the design control parameters in conventional SMC are $\Phi = 1$ and $\eta = 10$.

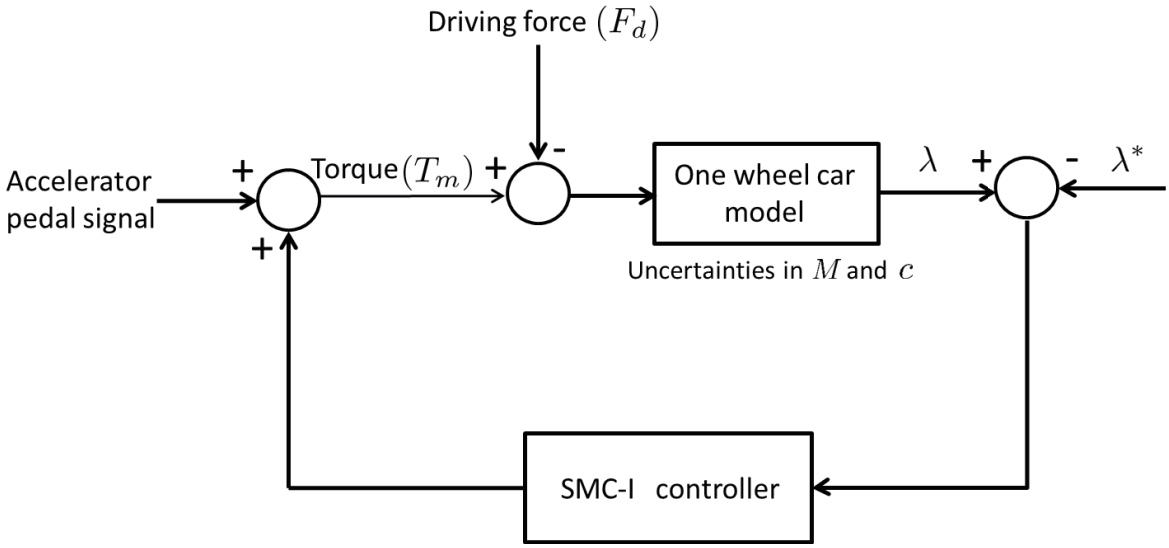

Figure 4.1 Block diagram of SMC-I control system

SMC-I control system in Simulations

As shown in Figure 4.1, the slip suppression control system using SMC-I is designed in simulation. The motor torque command includes two parts: the toque command generated by the accelerator pedal and the one from the slip suppression controller. The range of variation in the mass of the vehicle M and the road condition coefficient c are imposed as $M_{max} = 1400$[kg], $M_{min} = 1000$[kg], $c_{max} = 0.9$ and $c_{min} = 0.1$ respectively. So the nominal values of mass and road condition coefficient can be estimated as the arithmetic mean of the value of the bounds: $M_n = 1200$[kg] and $c_n = 0.5$.

Driver Model in Simulations

In simulations, it is thought that the driver's action controls the vehicle velocity generally. Based on the velocity desired in head, the driver makes a torque command by operating the accelerator pedal. As shown in Figure 4.2, there are two velocity controllers modeled with the simple primary delay elements for the driver's action. One is the velocity controller 1 which produces the main part of torque command by a feed forward control. The other one is the velocity controller 2 which makes a weak feedback of the error between the velocity command and the estimated vehicle velocity from the data of the speedometer or the scenery around the driver. In general EVs, the output torque command can be derived from this model and used as the motor torque command to the vehicle dynamics directly without any treatment. In comparison with the systems with other control methods, we call this method "**No control**" in simulations. The variable values in the velocity controller are given in Table 4.3.

As the input to the control system in the simulation by driver, the motor toque is generated by the constant pressure on the accelerator pedal, which depends on the desired vehicle velocity. Here, the vehicle velocity is desired to achieve 80[km] in 10[s] at a fixed acceleration after the vehicle starting off. We consider a case to simulate the road condition changing for this vehicle as follows. A vehicle stops at an intersection to wait for a green light on an icy road in winter. When the signal light has turned green, it accelerates to cross through the intersection. After a while, it enters into a wet asphalt road for a second, then runs on a dry asphalt road.

In order to verify the robustness of SMC-I with variation in the mass of the vehicle, here

we have made the variation in the mass by assigning the value of M to 1000[kg], 1100[kg], 1200[kg], 1300[kg] and 1400[kg] respectively. To show the robustness of SMC-I on various road conditions, three road surfaces are switching in the simulations, a icy road for the time from 0[s] to 8[s], an wet asphalt road from 8[s] to 9[s] and a dry asphalt road from 9[s] to 10[s].

Table 4.3 Values of velocity controller constants in the driver model

J_f	$(M_n r^2 + J_w)/r$
T_f	0.2
K_p	1.0
T_p	0.2

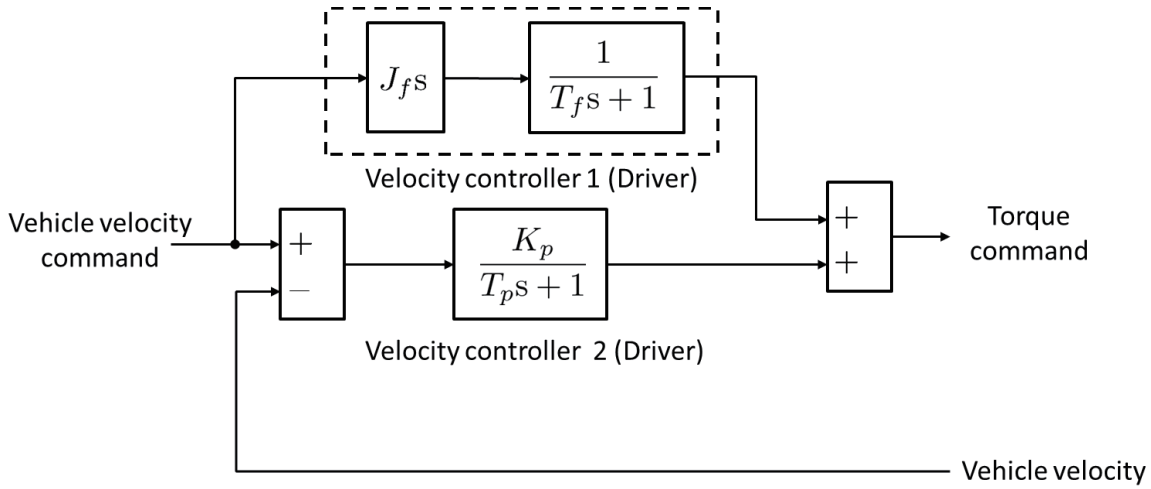

Figure 4.2 Block diagram of the velocity controller by driver

4.3.2 Simulation Results

Results of Robustness to the Variation in Mass and Road Condition

Figure 4.3 shows the responses of the slip ratio of vehicles with different masses on three switching road conditions. The slip ratio can converge to the reference value by the SMC-I method. It shows that SMC-I is robust to the variation existed in the mass of the vehicle.

At next, we compare SMC-I with conventional SMC and No control. Figures 4.4∼4.8 shows the responses of slip ratio and motor torque on three different road surfaces for five different masses respectively.

As shown in Figures 4.4(a)∼4.8(a), the responses of slip ratio with SMC-I can be suppressed at the reference value 0.13 accurately in a short time whenever the mass and road condition are both changing. For SMC-I, when the vehicle starts off on an icy road, the slip ratio rises fast because the value of motor torque is so high that the wheel turns spinning at

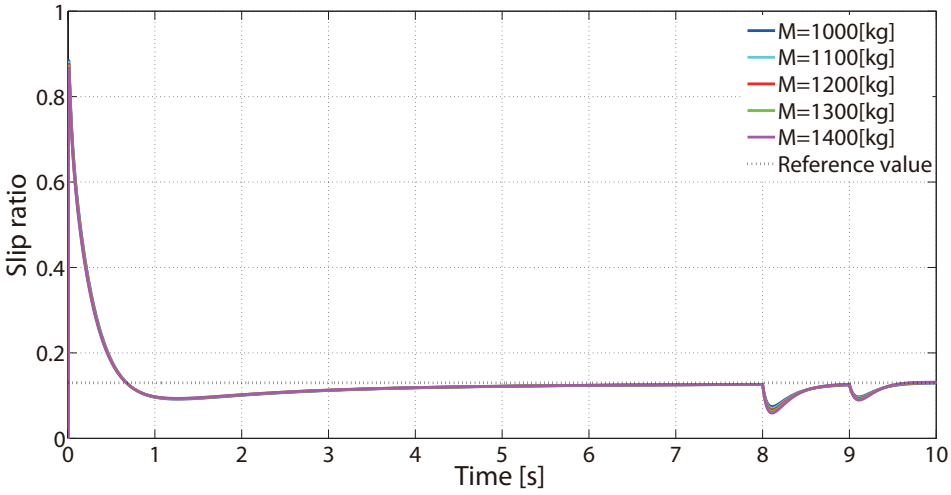

Figure 4.3 Time response of slip ratio with SMC-I for different vehicle masses

the beginning. By using slip ratio control, the motor torque is lowered, then the wheel velocity decreases to get a low value of slip ratio. As the vehicle runs on a wet road at 8[s], the decrease of wheel velocity is greater than the one of body velocity. This leads to the slip ratio dropping down at that point, then it returns to the reference value again. Likewise, the slip ratio decreases when the vehicle runs from wet asphalt road to dry asphalt road at 9[s], then converges to 0.13. The response with the conventional SMC can not converge to the reference value accurately because of the inherent steady state error. For No control, the slip ratio increases to a high value on the icy road because of large torque input making the wheel spinning. When the vehicle enters in a wet asphalt road and a dry asphalt road, the tire grip margin becomes larger than on an icy road, the slip ratio decreases rapidly.

Figures 4.4(b)$\sim$4.8(b) show the responses of the motor torque inputs of No control, SMC and SMC-I. For SMC-I and SMC, from 0[s] to 8[s] on the icy road, the torque value given at the start is so high that it grows rapidly in a very short time, then decreases at a low level to slow down the wheel velocity, which leading to a suitable tire grip margin. From 8[s] to 9[s] on the wet asphalt road, to achieve the maximum driving force, the torque keeps at a high level. During the last 1[s] on the wet asphalt road, the torque also reaches higher to achieve the maximum acceleration. Additionally, owing to the driver's desired vehicle velocity, the torque responses of No control have no change at the road surface switching spot.

From Figures 4.4$\sim$4.8, we can see that the responses of SMC-I have a high speed and precision to the reference value of slip ratio with respect to the torque than the conventional SMC. Furthermore, with the mass increasing, to meet the maximum acceleration, it is clear for SMC-I and conventional SMC that the values of motor torque also become large.

Results of Acceleration Performance

To estimate the acceleration performance of SMC-I, the responses of vehicle body velocity are shown in Figures 4.9∼4.13.

In each case, the vehicle with SMC-I achieves the best acceleration in 10[s] regardless of changing of road conditions. This is why the vehicle with SMC attains the maximum driving force by suppressing the slip ratio to the reference value. The vehicle with No control has loss of driving force owing to the wheel spinning on the icy road. Besides, the slip ratio can not be suppressed to the reference value, which results in that the vehicle does not get the maximum driving force on the dry asphalt road and wet asphalt road in this simulation.

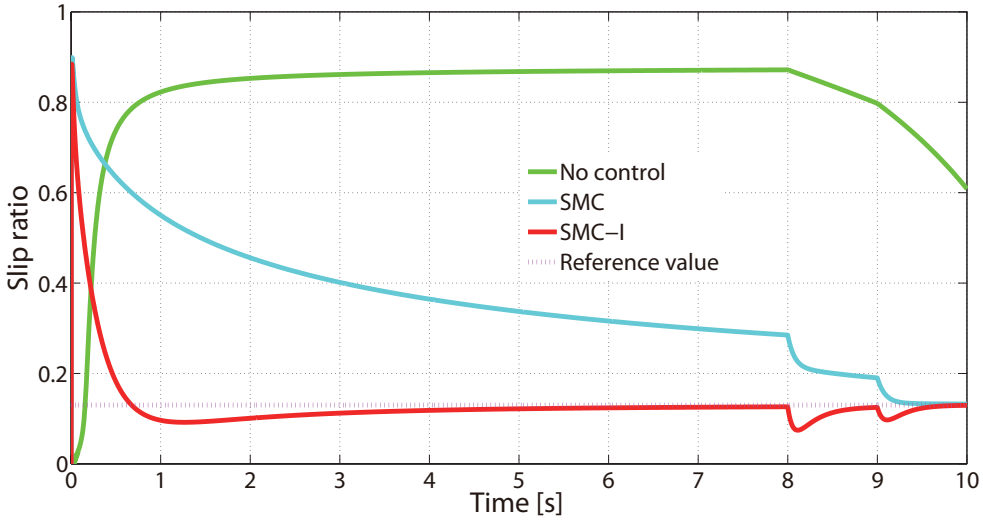

(a) Slip ratio

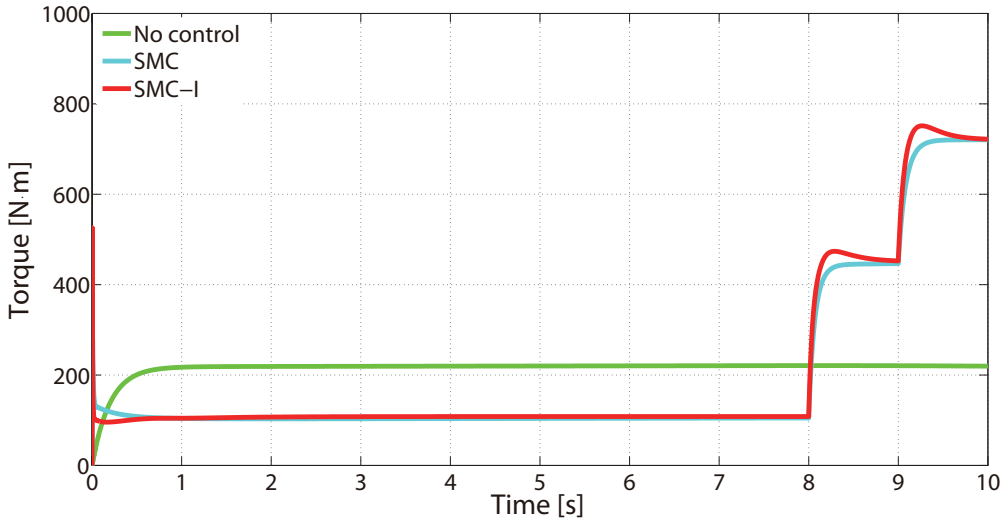

(b) Motor torque

Figure 4.4 Simulation results of No control, SMC and SMC-I ($M = 1000$[kg])

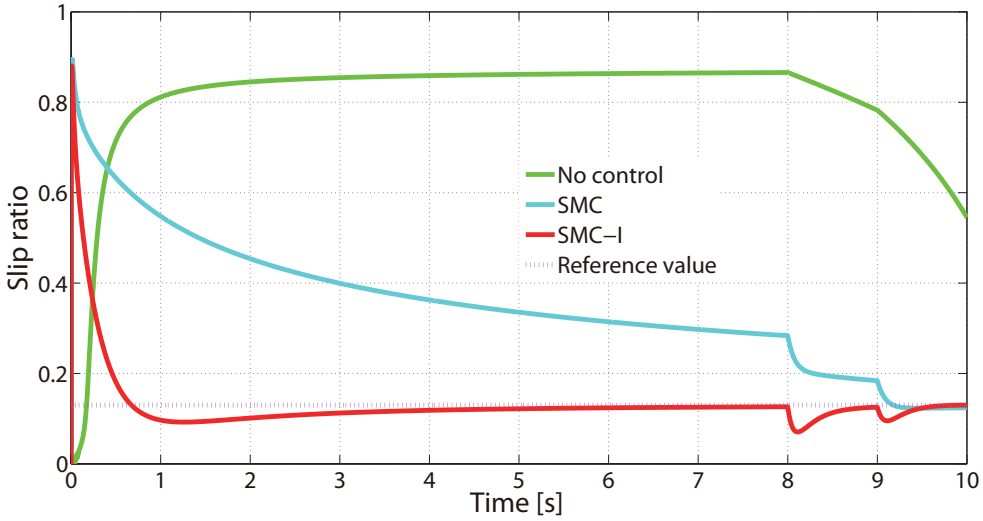

(a) Slip ratio

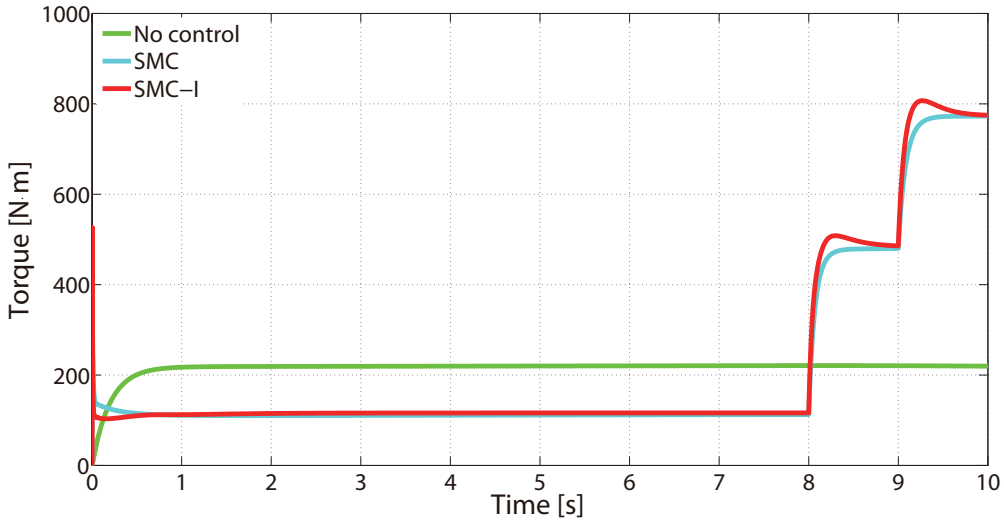

(b) Motor torque

Figure 4.5 Simulation results of No control, SMC and SMC-I ($M = 1100$[kg])

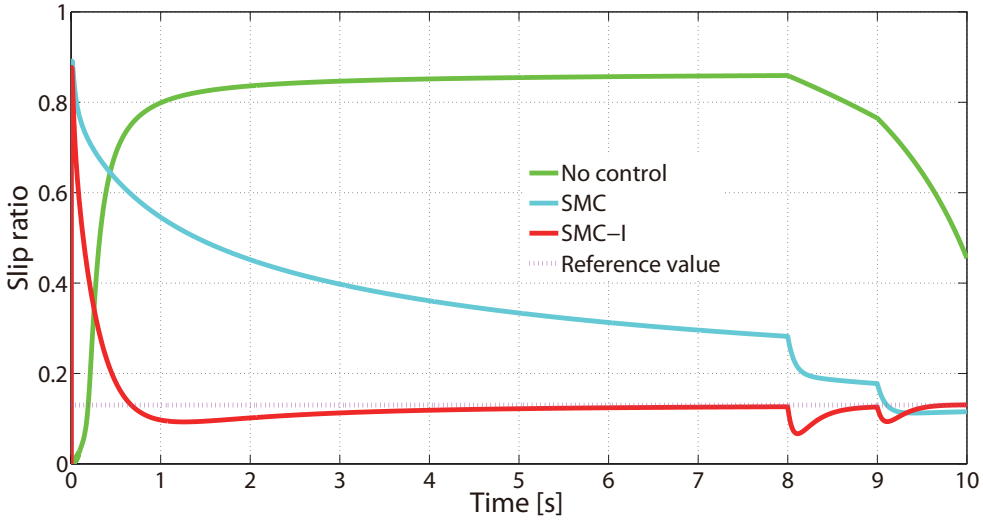

(a) Slip ratio

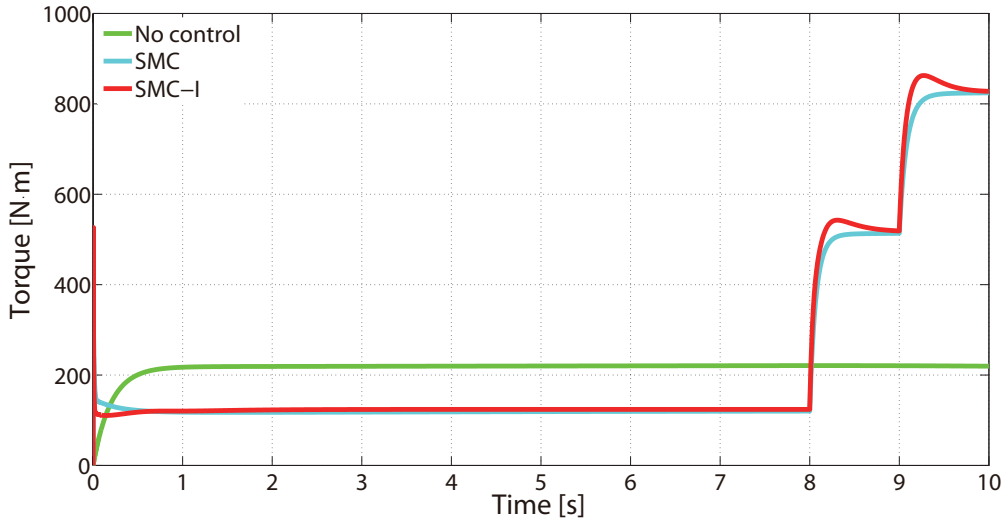

(b) Motor torque

Figure 4.6 Simulation results of No control, SMC and SMC-I ($M = 1200$[kg])

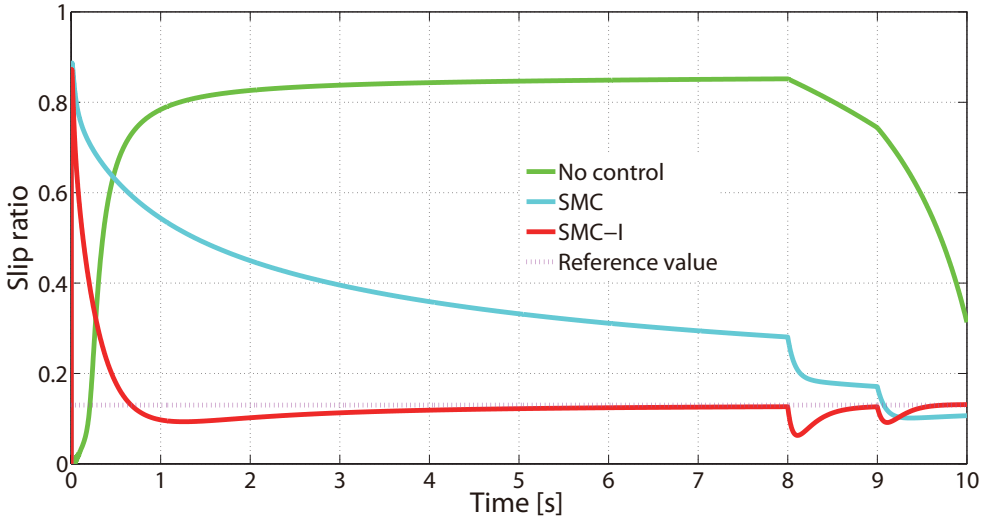

(a) Slip ratio

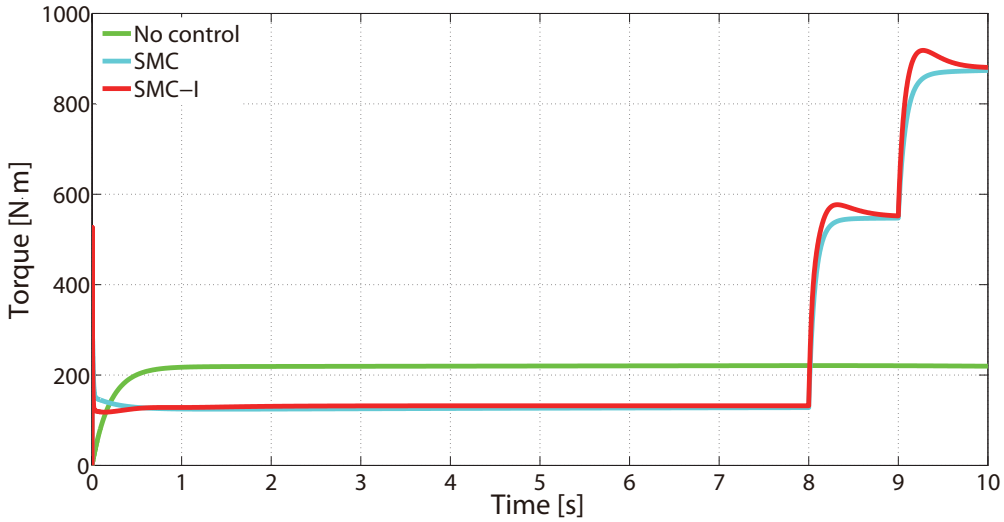

(b) Motor torque

Figure 4.7 Simulation results of No control, SMC and SMC-I ($M = 1300$[kg])

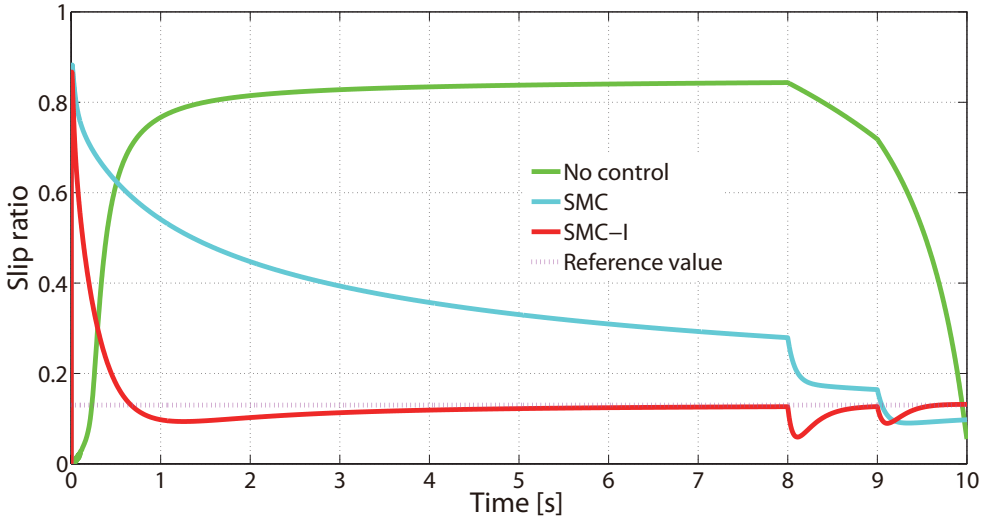

(a) Slip ratio

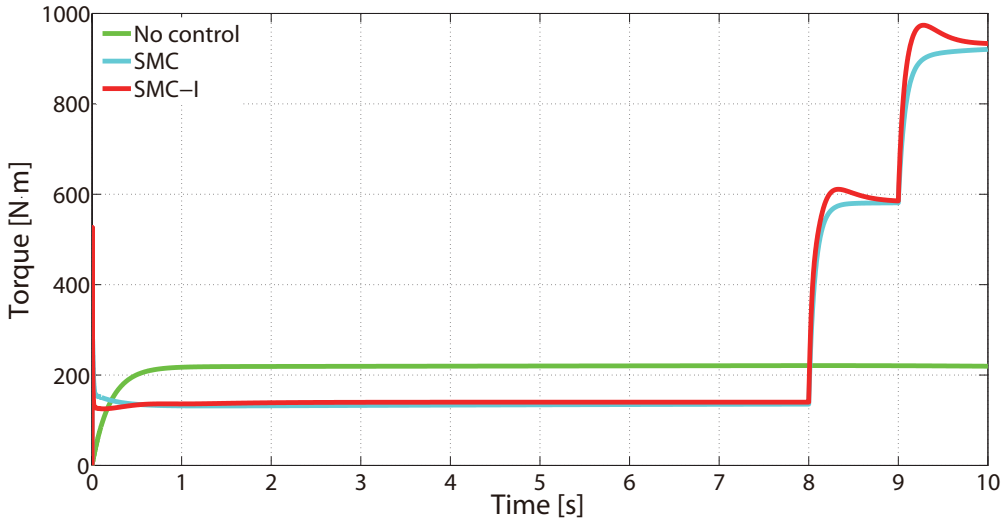

(b) Motor torque

Figure 4.8 Simulation results of No control, SMC and SMC-I ($M = 1400$[kg])

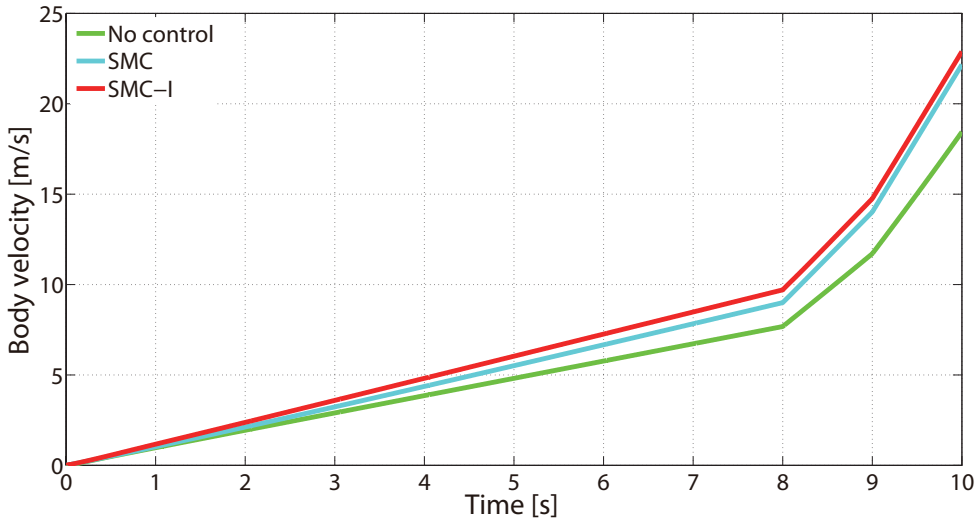

Figure 4.9 Time response of body velocity with No control, SMC and SMC-I ($M = 1000$[kg])

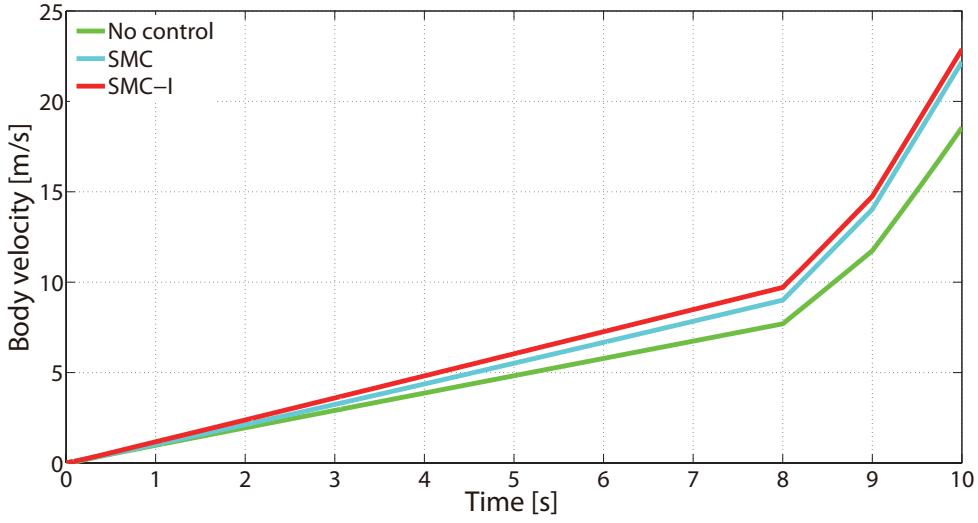

Figure 4.10 Time response of body velocity with No control, SMC and SMC-I ($M = 1100$[kg])

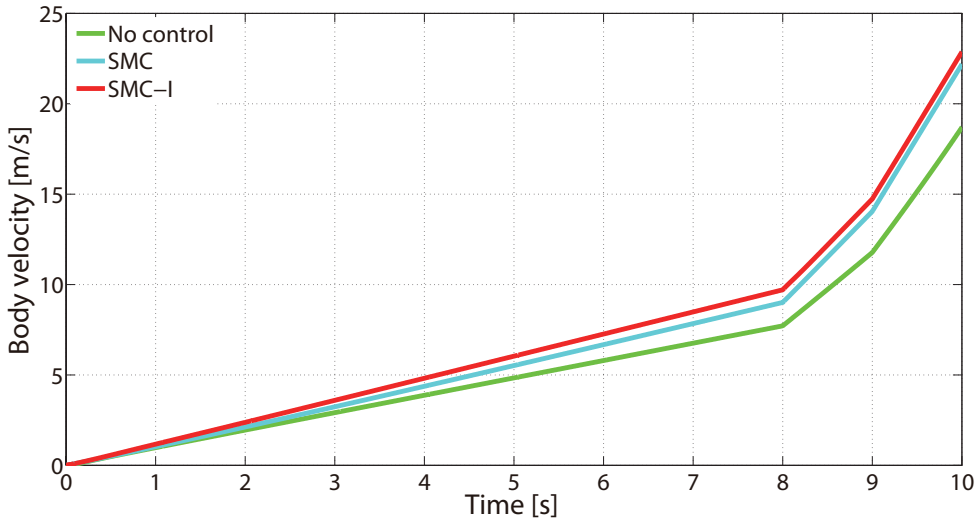

Figure 4.11 Time response of body velocity with No control, SMC and SMC-I ($M = 1200$[kg])

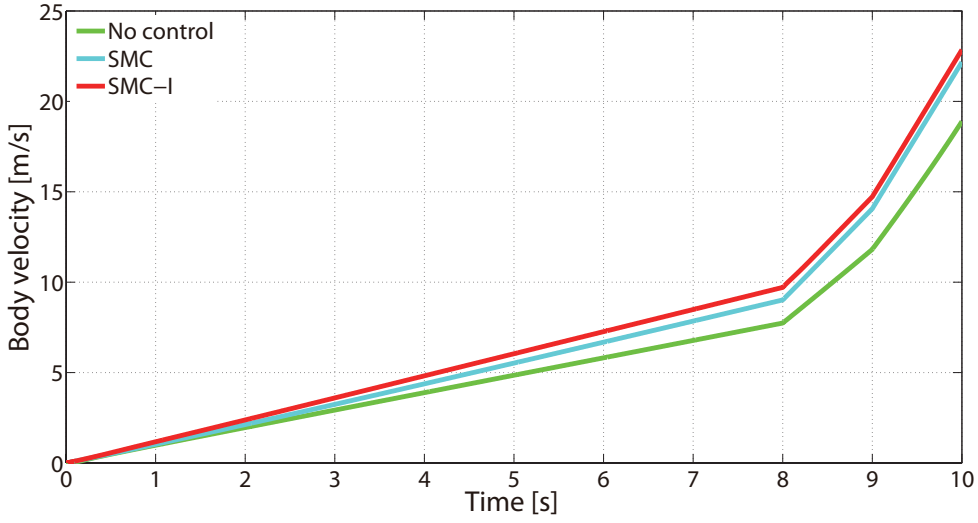

Figure 4.12 Time response of body velocity with No control, SMC and SMC-I ($M = 1300$[kg])

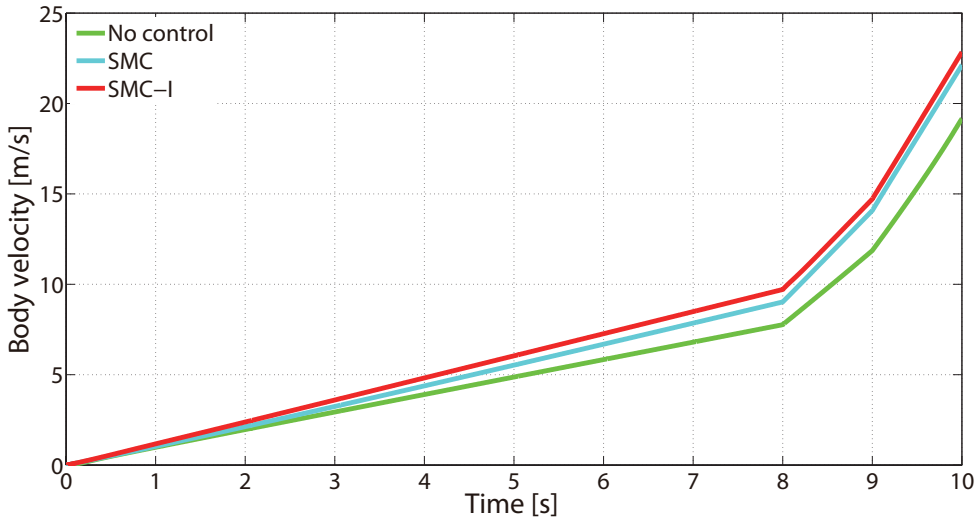

Figure 4.13 Time response of body velocity with No control, SMC and SMC-I ($M = 1400$[kg])

Results of Energy Conservation Performance

Generally, it is not easy to estimate the energy consumption accurately without measurement by experiments on the actual vehicle. In this dissertation, we estimate the energy consumption of the vehicle by calculating the energy consumed by the electric motor. In order to estimate the energy consumption of the motor, as a beginning, we give the energy consumed to drive the wheel to rotation based on the following two assumptions:

Assumption 1

The electric energy is all utilized to drive the wheel and the extra heat is neglected.

Assumption 2

The energy consumed by the vehicle is approximately equated to the work of the torque.

Under these assumptions, the work W_r done by the torque T_m on the wheel is used to represent the consumed energy E_r and it is given by

$$E_r = W_r = \int_0^{t_s} T_m(t)\omega(t)dt. \tag{4.31}$$

where t_s is the simulation time.

In the simulations, the total distance D_d is calculated by integrating the vehicle body velocity from 0 to t_s and is defined as

$$D_d = \int_0^{t_s} V(t)dt. \tag{4.32}$$

To learn how much the energy consumed with respect to the distance, the energy consumption rate (the average energy cost per meter) E_p is used to evaluate the energy consumption performance in simulations. E_p is defined by

$$E_p = \frac{E_r}{D_d}. \tag{4.33}$$

To confirm the energy conservation performance by SMC-I, we compare it with conventional SMC and No control. Tables 4.4∼4.8 show the results of the energy consumption rate in the cases of different vehicle masses. We can see that SMC-I has the minimum average energy consumption rate in each case. That is, SMC-I can minimize the energy loss by suppressing the wheel slip. For No control, the amount of energy cost decreases because of suppressing the wheel slip by an increment of mass to do grip the road well. Conversely, the amount of energy cost for SMC-I and SMC increases with the mass growth which also implies that an EV should be made as light as possible to save more energy.

Table 4.4 Results of energy consumption rate with No control, SMC and SMC-I ($M = 1000$[kg])

	E_r [Wh]	D_d [m]	E_p [Wh/km]
No control	80.34	55.52	1447
SMC	28.30	64.82	437
SMC-I	28.11	69.58	404

Table 4.5 Results of energy consumption rate with No control, SMC and SMC-I ($M = 1100$[kg])

	E_r [Wh]	D_d [m]	E_p [Wh/km]
No control	76.03	55.67	1366
SMC	30.13	64.87	464
SMC-I	30.15	69.58	433

Table 4.6 Results of energy consumption rate with No control, SMC and SMC-I ($M = 1200$[kg])

	E_r [Wh]	D_d [m]	E_p [Wh/km]
No control	71.67	55.85	1283
SMC	31.89	64.92	491
SMC-I	32.18	69.57	463

Table 4.7 Results of energy consumption rate with No control, SMC and SMC-I ($M = 1300$[kg])

	E_r [Wh]	D_d [m]	E_p [Wh/km]
No control	67.25	56.07	1199
SMC	33.55	64.96	516
SMC-I	34.21	69.55	492

Table 4.8 Results of energy consumption rate with No control, SMC and SMC-I ($M = 1400$[kg])

	E_r [Wh]	D_d [m]	E_p [Wh/km]
No control	62.75	56.33	1114
SMC	35.10	64.98	540
SMC-I	36.22	69.54	521

4.4 Summary

This chapter proposed an extended SMC method by adding the integral term to the sliding function (SMC-I) for improving the performance of the slip ratio control for EVs. The control objective focused on suppressing the slip ratio to the reference value within the specified variation in mass of vehicle and road conditions which allowed the vehicle to get the maximum driving force and minimum energy cost during acceleration.

As numerical examples of the one wheel model, the simulations using SMC-I method were executed, and the robustness to the uncertainties in the vehicle mass and the road conditions was verified. Additionally, by comparing with SMC and No control, the vehicle with SMC-I performed good acceleration performance with low energy consumption rate.

In this chapter, the gain K_{in} of integral action added in the sliding function was determined as a constant by trial and error. The problem which we have to consider next is what can be done to develop a systematic method to find the optimal value of K_{in} on time. In next chapter, this problem will be addressed.

Chapter 5

SMC with Integral Action Based on Model Predictive Control

5.1 Introduction

For the SMC-I controller described in chapter 4, the control law is a function of the integral gain K_{in}, which has been determined by trial and error. It is difficult to manually determine the parameter K_{in} that yields optimal controller performance. Other than that, the parameter determined for one initial condition can yield poor or unacceptable performance for other different initial conditions. The question we have to ask here is what should be done to develop a method to determine K_{in} effectively. MPC is a class of control algorithm in which the current control action is obtained by solving an optimal control problem on-line. In this chapter, the SMC-I method based on model predictive control (MP-SMC-I) is presented to

adjust K_{in} optimally.

MPC predicts the future state behavior based on past and current values and on the proposed optimal future control actions by using a controlled object model. These control actions are calculated by the optimizer taking into account the objective function as well as the constraints, only the first control input is considered as the controlled object then repeated.

We give a simple example to explain the basic MPC strategy here. Consider a SISO linear discrete time system, modeled by

$$x(k+1) = ax(k) + bu(k) \tag{5.1}$$

$$y(k) = cx(k). \tag{5.2}$$

where $x(k) \in R$ is the state, $u(k) \in R$ is the control input, $y(k) \in R$ is the output, and k represents the current time. The system coefficients a, b and c are scalars.

The basic MPC strategy is shown in Figure 5.1. "ˆ" denotes the predicted values and this notation is used in this and following sections. The control objective is to make the control output $y(t)$ converge to the reference value r. The future outputs for a determined horizon N, called the prediction horizon, are predicted at each time step using the control model. These predicted outputs $\hat{y}(k+i)$ for $i = 1, \cdots, N$ depend on the known values of past inputs and outputs and on the future control inputs $\hat{u}(k+i)$, $i = 0, \cdots, N-1$.

The MPC algorithm is described as following steps:

Step 1. Estimate the parameters of a model by measuring the value of state variable $x(k)$ at the current time k.

Step 2. Compute the future control input sequence $\hat{u}(k+0), \cdots, \hat{u}(k+N-1)$ by optimizing

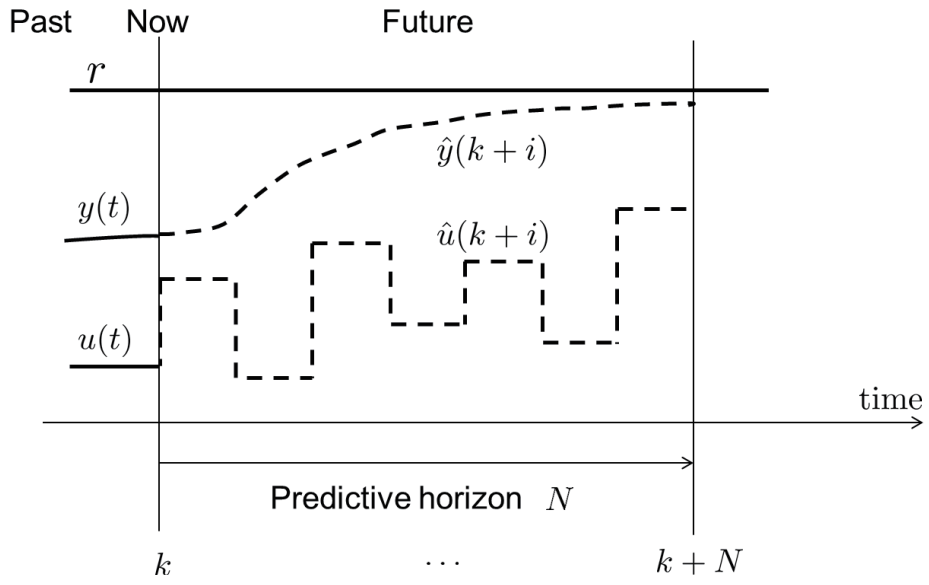

(a) At time k

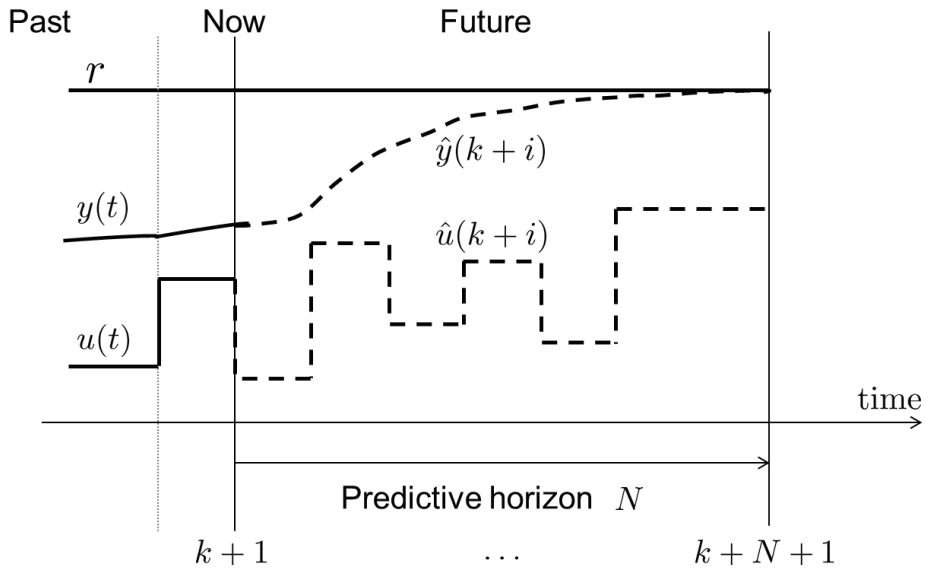

(b) At time $k+1$

Figure 5.1 Graphical interpretation of basic MPC strategy

a determined criterion to keep the output as close as possible to the reference value r during the prediction horizon.

Step 3. Only the first control input $\hat{u}(k+0)$ of the sequence obtained at step 2 is sent to the system and to be calculated. Then returning to step 1 and repeating with the new value and all the sequences are brought up to date.

The MPC algorithm is executed repeatedly by solving an optimization problem step by step in the prediction, which is called receding horizon principle and it is one of the central ideas of MPC. So in this chapter, we determine the parameter K_{in} based on the MPC algorithm.

5.2 SMC with Integral Action Based on MPC Algorithm

5.2.1 Discrete Time State Space Model

Generally, a MPC algorithm is used to predict the future state behavior base on the discrete-time state space model. The continuous time state space model for the slip ratio control represented by Equation (4.1) in chapter 4 can not be dealt with in the same way. It is transformed to the discrete time state space model at sampling time $t = kT$, T is the sampling period. The torque input is defined by

$$T_m(t) = T_m(kT),\ kT \leq t < (k+1)T. \tag{5.3}$$

For convenience, we will omit T in the following equations.

The controlled object of vehicle dynamics can be described by a nonlinear deference equa-

tion as follows.

$$\lambda(k+1) = f_d\big(k, \lambda(k)\big) + b_d\big(k, \lambda(k)\big)T_m(k) \tag{5.4}$$

where $\lambda(k)$ is the state variable representing the slip ratio at time k. $f_d\big(k, \lambda(k)\big)$ describes the nonlinearity of the discrete time system, $b_d\big(k, \lambda(k)\big)$ is the input gain, and they are give by

$$f_d\big(k, \lambda(k)\big) = -\frac{g}{V_w(k)}\left\{1 + \big[1 - \lambda(k)\big]\frac{r^2 M}{J_w}\right\}\mu\big(c, \lambda(k)\big) \tag{5.5}$$

$$b_d\big(k, \lambda(k)\big) = \frac{\big[1 - \lambda(k)\big]r}{J_w V_w(k)}. \tag{5.6}$$

The control input $T_m(t)$ given by Equation (4.29) can be rewritten as

$$\begin{aligned} T_m(k) = \frac{1}{b_d\big(k, \lambda(k)\big)}\Bigg\{ & f_{dn}\big(k, \lambda(k)\big) - K_{in}(k)\big[\lambda(k) - \lambda^*\big] \\ & - \big[F_d\big(k, \lambda(k)\big) + \eta\big]\text{sat}\left(\frac{s\big(k, \lambda(k), K_{in}(k)\big)}{\Phi}\right)\Bigg\} \end{aligned} \tag{5.7}$$

where λ^* is the reference slip ratio, η is the design parameter, and both of them are constants. $f_{dn}\big(k, \lambda(k)\big)$ is the estimation of $f_d\big(k, \lambda(k)\big)$ and is defined as

$$f_{dn}\big(k, \lambda(k)\big) = -\frac{g}{V_w(k)}\left\{1 + \big[1 - \lambda(k)\big]\frac{r^2 M_n}{J_w}\right\}\mu\big(c_n, \lambda(k)\big). \tag{5.8}$$

$F_d\big(k, \lambda(k)\big)$ is can be rewritten from Equation (4.15) by

$$\begin{aligned} F_d\big(k, \lambda(k)\big) = \frac{g}{\Big|V_w\big(k, \lambda(k)\big)\Big|}\Bigg\{ & \Big|\mu\big(c_{max}, \lambda(k)\big) - \mu\big(c_n, \lambda(k)\big)\Big| \\ & + \big(1 - \lambda(k)\big)\frac{r^2}{J_w}\Big|M_{max}\mu\big(c_{max}, \lambda(k)\big) - M_n\mu\big(c_n, \lambda(k)\big)\Big|\Bigg\}. \end{aligned} \tag{5.9}$$

5.2.2 Derivation of Predicted Model

Now, we set current time to k. For a prediction horizon H_p, the predicted slip ratios $\hat{\lambda}(k+i)$ for $i = 1, \cdots, H_p$ depend on the known values of current slip ratios, current torque input and future torque inputs. By using Equation (5.4), the predicted slip ratios can be represented as

$$\begin{cases} \hat{\lambda}(k+1) &= f_d\big(k, \lambda(k)\big) + b_d\big(k, \lambda(k)\big)\hat{T}_m(k) \\ \hat{\lambda}(k+2) &= f_d\big(k+1, \hat{\lambda}(k+1)\big) + b_d\big(k+1, \hat{\lambda}(k+1)\big)\hat{T}_m(k+1) \\ &\vdots \\ \hat{\lambda}(k+H_p) &= f_d\big(k+H_p-1, \hat{\lambda}(k+H_p-1)\big) \\ &\quad + b_d\big(k+H_p-1, \hat{\lambda}(k+H_p-1)\big)\hat{T}_m(k+H_p-1) \end{cases} \tag{5.10}$$

where $\hat{T}_m(k+i)$, $i = 0, \cdots, H_p - 1$ are predicted control inputs. $\hat{T}_m(k+i)$ is given by

$$\begin{aligned} \hat{T}_m(k+i) = \frac{1}{b_d\big(k+i, \hat{\lambda}(k+i)\big)} \Big\{ & f_{dn}\big(k+i, \hat{\lambda}(k+i)\big) - K_{in}\big[\hat{\lambda}(k+i) - \lambda^*\big] \\ & - \big[F_d\big(k+i, \hat{\lambda}(k+i)\big) + \eta\big] \text{sat}\left(\frac{s\big(k+i, \hat{\lambda}(k+i), K_{in}\big)}{\Phi} \right) \Big\}. \end{aligned} \tag{5.11}$$

5.2.3 Calculation of Parameter K_{in}

For the slip suppression control, on one hand, in order to obtain large driving force, the slip ratio is need to be close as possible to the reference slip ratio, on the other hand, the torque considered as the energy consumed here increases, which is not expected. Therefore, the objective function takes a form of a weighted absolute sum of errors between the predicted slip ratio and the reference slip ratio, and the predicted torque inputs. The objective function

J is defined as follows:

$$J = \sum_{i=0}^{H_p-1} \left\{ q|\hat{\lambda}(k+i+1) - \lambda^*| + r|\hat{T}_m(k+i)| \right\} \tag{5.12}$$

where q, r are the positive weights. By using Equations (5.10) and (5.11), both $\hat{\lambda}$ and $\hat{T}_m$ can be expressed by K_{in}, thus J can be represented by a function of K_{in}. Our aim is to find the parameter K_{in} that minimizes this objective function $J(K_{in})$. In a nutshell, the optimization problem is given by

$$\min_{K_{in}} J(K_{in}) \tag{5.13}$$

$$\text{s.t. Equations (5.10) and (5.11)}$$

$$i = 0, \cdots, H_p - 1.$$

At time k, the optimal $K_{in}(k)$ can be found by solving Equation (5.14) with some optimization method (here, a grid search method is made to the discretized K_{in}). Once the optimal $K_{in}(k)$ is determined, it is used as the continuous $K_{in}(t)$ for $kT \leq t < (k+1)T$, then the continuous control input $T_m(t)$ can be calculated by Equation (4.1). At the next sampling time $k+1$, the optimal $K_{in}(k+1)$ is calculated as the previous step. At each sampling period, the same operation is repeated. Therefore, using the MP-SMC-I method could determine the optimal parameter K_{in} by solving the optimization problem.

5.3 Simulation Examples

In this section, the simulation example is made to verify the effectiveness of the MP-SMC-I method for the slip suppression control in acceleration. The performance of the MP-SMC-I

method in this dissertation is compared with that of No control, SMC and SMC-I method.

5.3.1 Simulation Setup

The simulation environment is similar to the one using in chapter 4. The vehicle parameter values listed in Table 4.2 are used in this section.

MP-SMC-I Control System in Simulations

The block diagram of slip suppression control system using MP-SMC-I is shown in Figure 5.2. The motor torque command includes the torque produced by the driver and the one by the slip suppression controller. In the controller design, the uncertainties in the actual mass of vehicle and real road conditions should be taken into account to meet the control performance. Here, the range of the uncertainties in the mass of vehicle M is $[1000, 1400]$[kg] and the range of road condition coefficient c is $[0.1, 0.9]$. The nominal values used in the controller design taking the arithmetic mean of the edge values are $M_n = 1200$[kg], $c_n = 0.5$.

For verifying the robustness of MP-SMC-I when the vehicle runs on various road surfaces, three road surfaces switch in the simulation by time as: an icy road during $[0, 8)$[s], a wet asphalt road during $[8, 9)$[s] and a dry asphalt road during $[9, 10]$[s]. In each simulation, the mass of vehicle changes to confirm the robustness of MP-SMC-I to the uncertainties in mass as well.

The driver model of simulations in chapter 4 shown in Figure 4.2 is also used here. The vehicle body velocity is desired to get 80[km] in 10[s] by a fixed acceleration after the car starting off on the icy road surface from still, where the driver pulling a constant pressure on

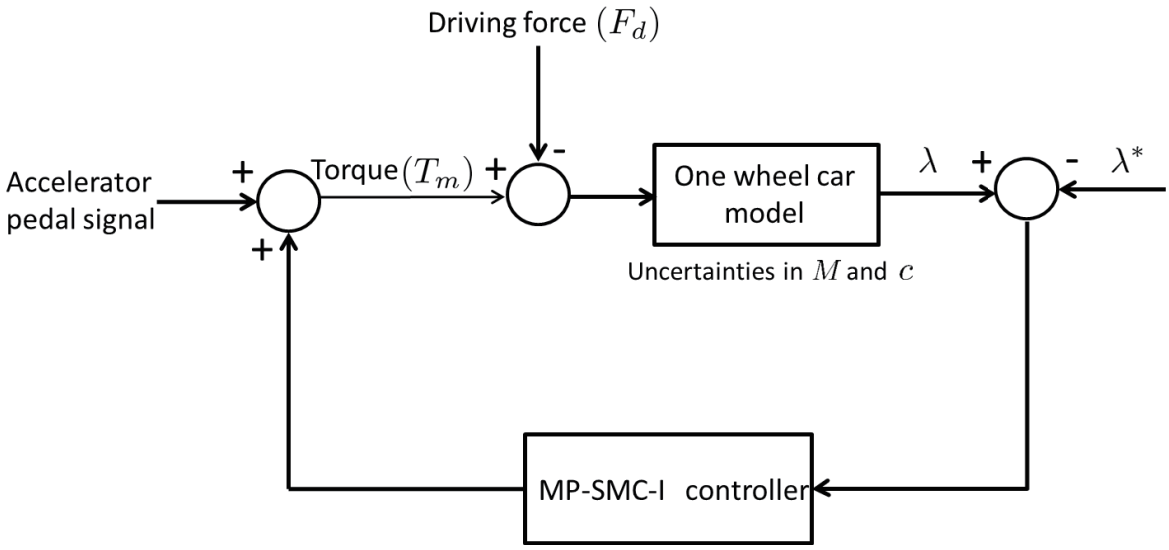

Figure 5.2 Block diagram of MP-SMC-I control system

the accelerator pedal produces the motor torque. The values of velocity controller constants in the driver model listed in Table 4.3

Configurations of Controller Parameters

The controller parameters Φ, η as well as the integral gain K_{in} are listed in Table 5.1. The same values of K_{in} used in SMC and SMC-I are determined by trial and error, which are used in the simulation example in chapter 4. The value of K_{in} was adjusted with one increment ΔK_{in} in the range of $[0, 200]$. The weights q and r are also determined by trial and error in this simulation.

Table 5.1 Configurations of the controllers: SMC, SMC-I and MP-SMC-I

SMC	$\Phi = 1, \eta = 10$ $K_{in} = 0$
SMC-I	$\Phi = 1, \eta = 10$ $K_{in} = 6$
MP-SMC-I	$\Phi = 1, \eta = 10$ $0 \leq K_{in} \leq 200, \Delta K_{in} = 1$ $q = 1.0 \times 10^8$ $r = 1.0$

5.3.2 Simulation Results

Results of Robustness to the Variation in Mass and Road Condition

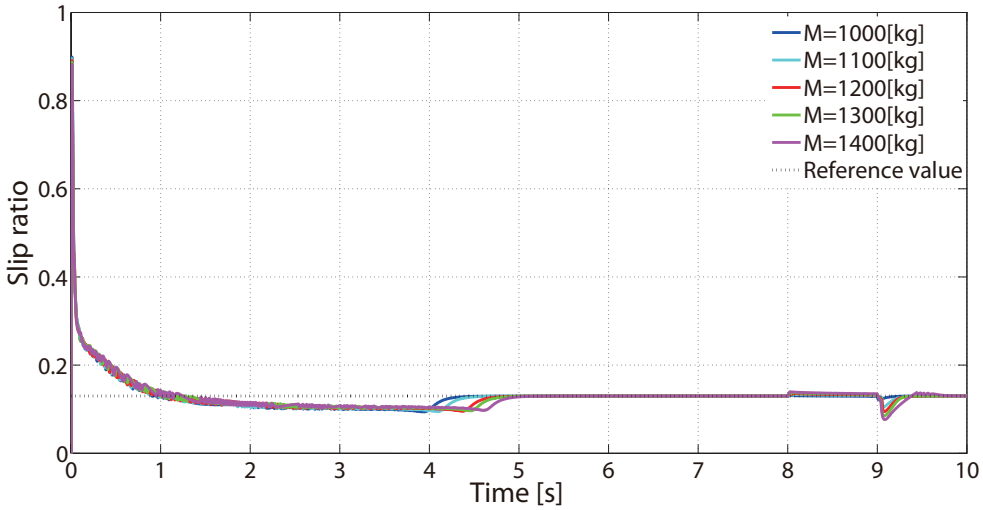

Figure 5.3 Time response of slip ratio with MP-SMC-I for different vehicle masses

As shown in Figure 5.3, the slip ratio can be suppressed to reference value 0.13 represented by black dot line accurately and rapidly regardless of the masses changing by 100[kg] from 1000[kg] to 1400[kg]. This implies that MP-SMC-I acts robustly to the variation in vehicle mass. It also makes a good transient performance at the switching spots on the road condition.

Figures 5.4(a)$\sim$5.8(a) show the responses of slip ratio under three different road conditions for five different cases of mass: 1000[kg], 1100[kg], 1200[kg], 1300[kg] and 1400[kg]. The slip ratio by MP-SMC-I can be suppressed to the reference value more accurately and rapidly than SMC-I. When the road condition changes, the slip ratio by MP-SMC-I also keep an suitable transient performance, reducing the steady state error and rising time. As shown in Figures 5.4(b)$\sim$5.8(b), the motor torque utilized by MP-SMC-I sufficiently to drive the wheel. The fluctuation in torque occurs at the time of road condition switching, which leads to K_{in} setting based on the prediction in the set prediction interval by the MPC algorithm. K_{in} is adjusted on-line for the optimum value from the objective function during the prediction interval when the road condition switches.

In Figures 5.9$\sim$5.13, the response of K_{in} varies sharply at the road condition switching spot because the tire grip margin changes, which leading to adjust K_{in} to achieve the sufficient driving force. Once the slip ratio deviates from the reference value, K_{in} is adjusted much based on MPC algorithm to get the appropriate force to drive the wheel to reach the reference value finally.

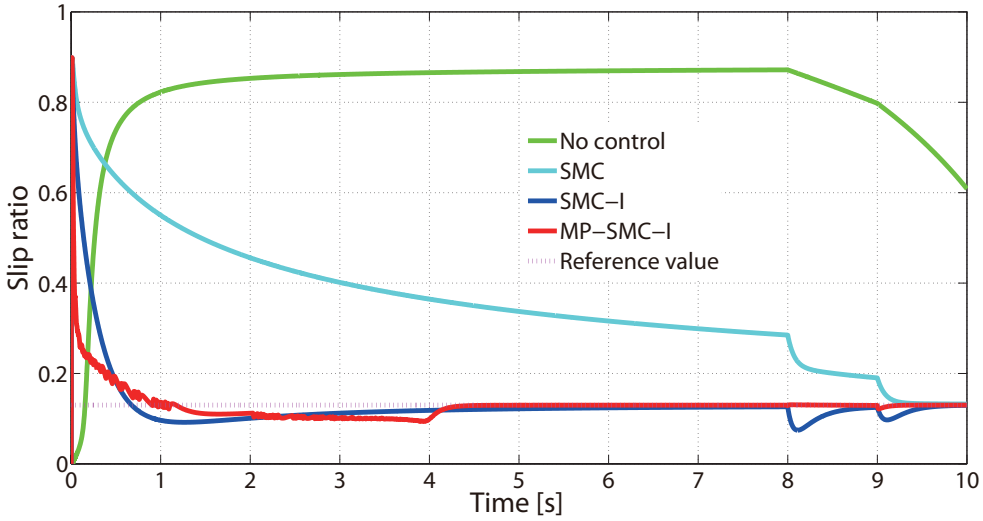

(a) Slip ratio

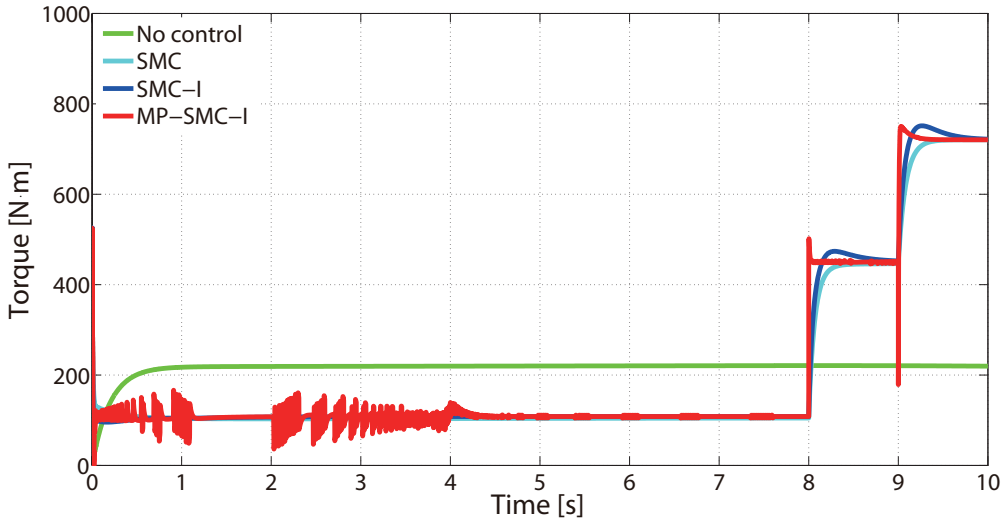

(b) Motor torque

Figure 5.4 Simulation results with No control, SMC, SMC-I and MP-SMC-I ($M = 1000$[kg])

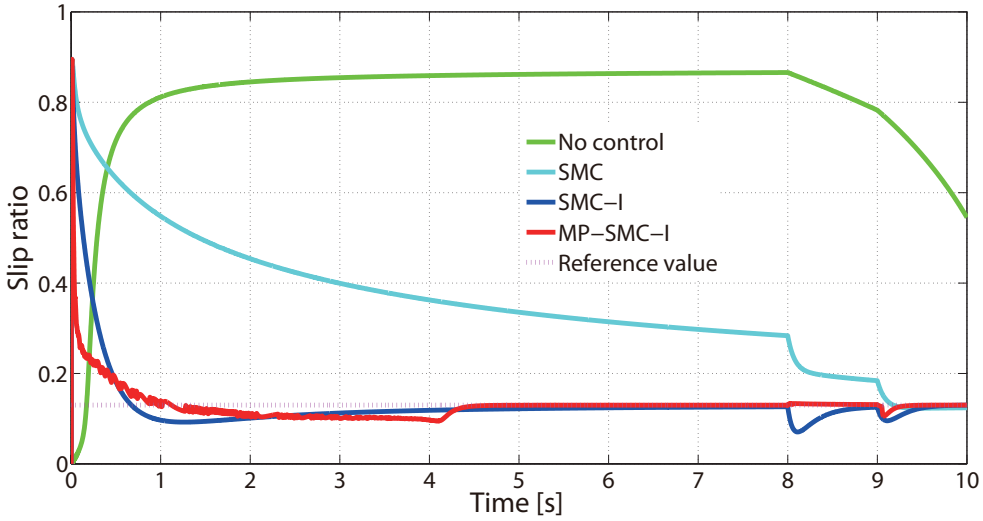

(a) Slip ratio

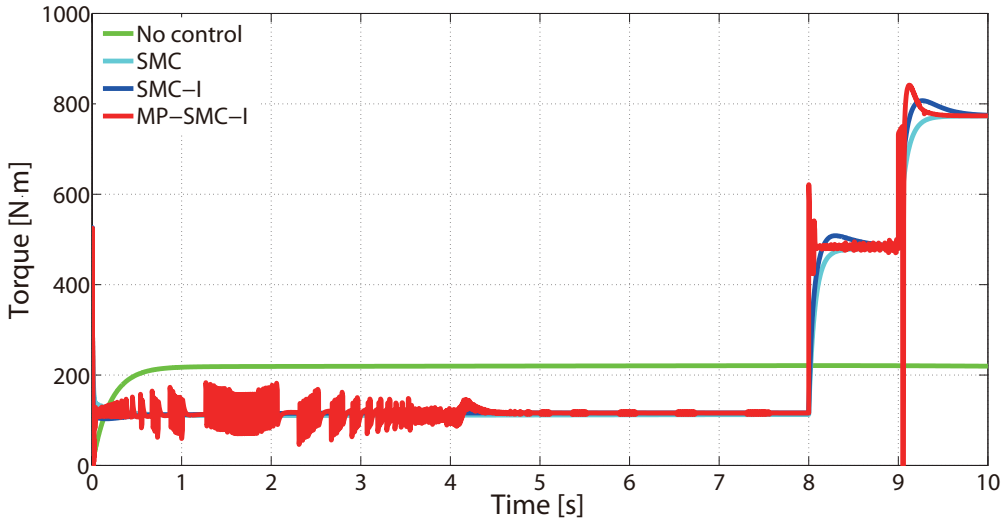

(b) Motor torque

Figure 5.5 Simulation results with No control, SMC, SMC-I and MP-SMC-I ($M = 1100$[kg])

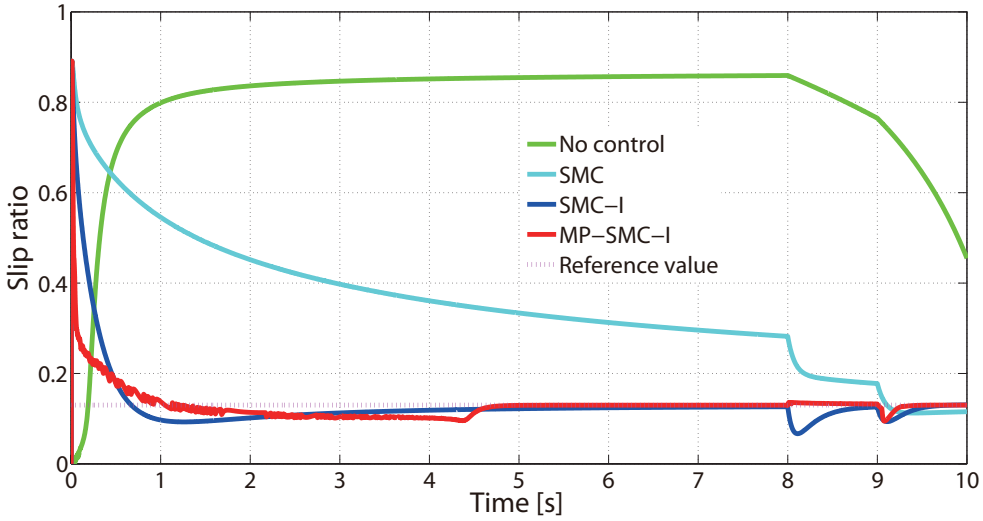

(a) Slip ratio

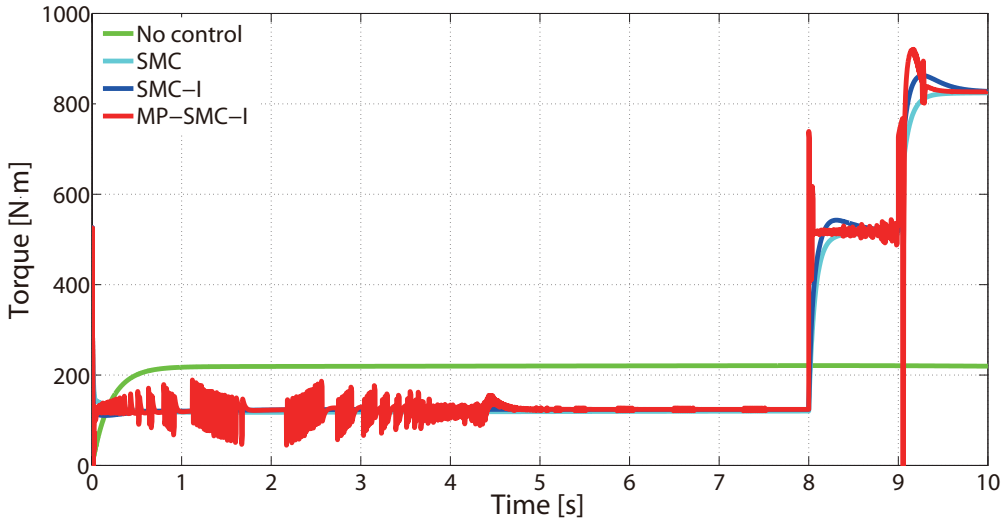

(b) Motor torque

Figure 5.6 Simulation results with No control, SMC, SMC-I and MP-SMC-I ($M = 1200$[kg])

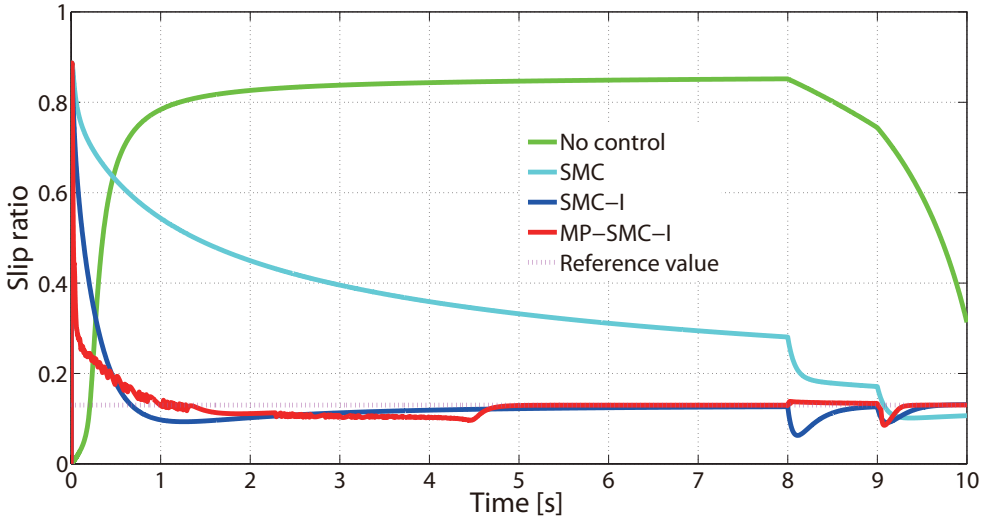

(a) Slip ratio

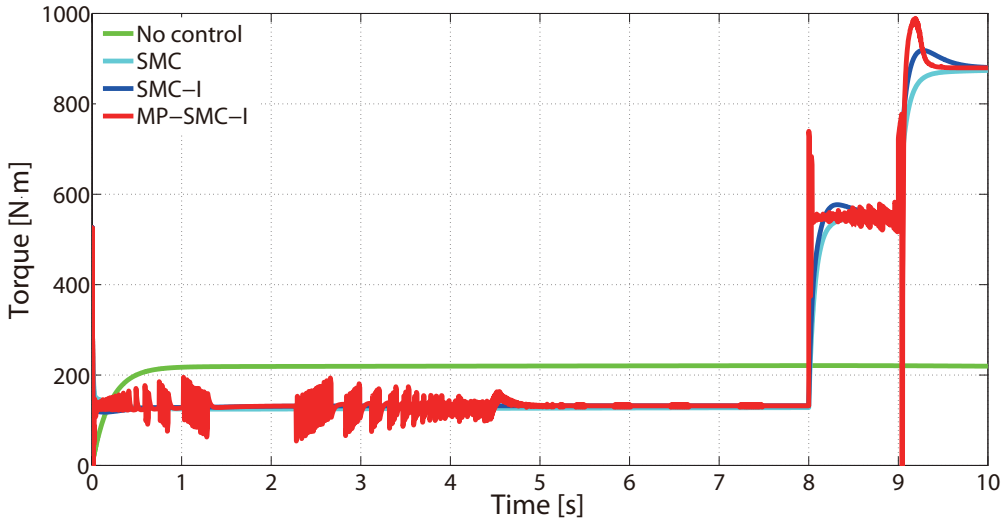

(b) Motor torque

Figure 5.7 Simulation results with No control, SMC, SMC-I and MP-SMC-I ($M = 1300$[kg])

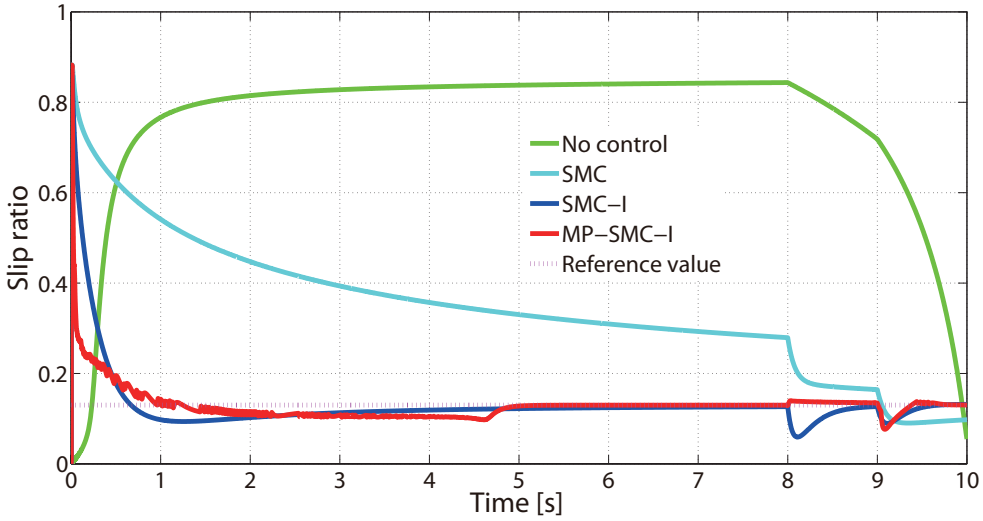

(a) Slip ratio

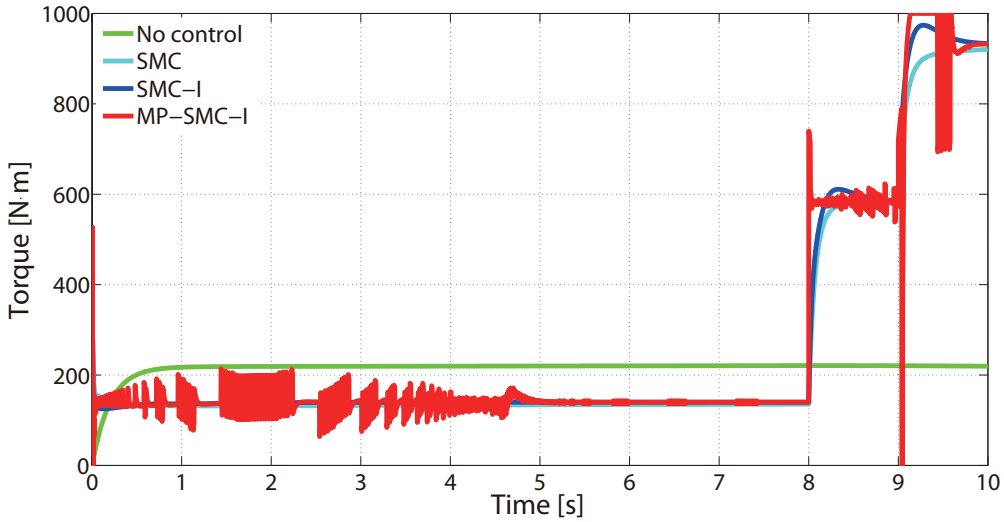

(b) Motor torque

Figure 5.8 Simulation results with No control, SMC, SMC-I and MP-SMC-I ($M = 1400$[kg])

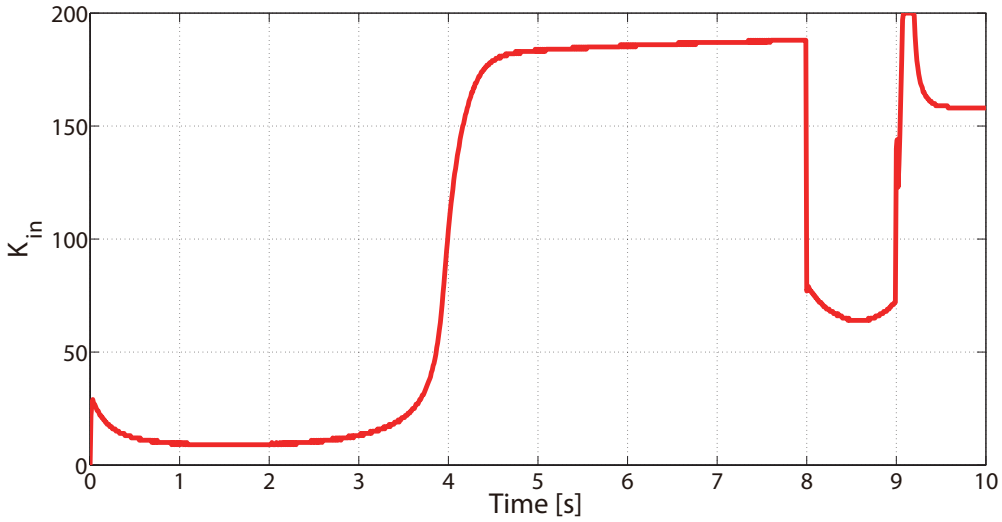

Figure 5.9 Time response of K_{in} for MP-SMC-I ($M = 1000$[kg])

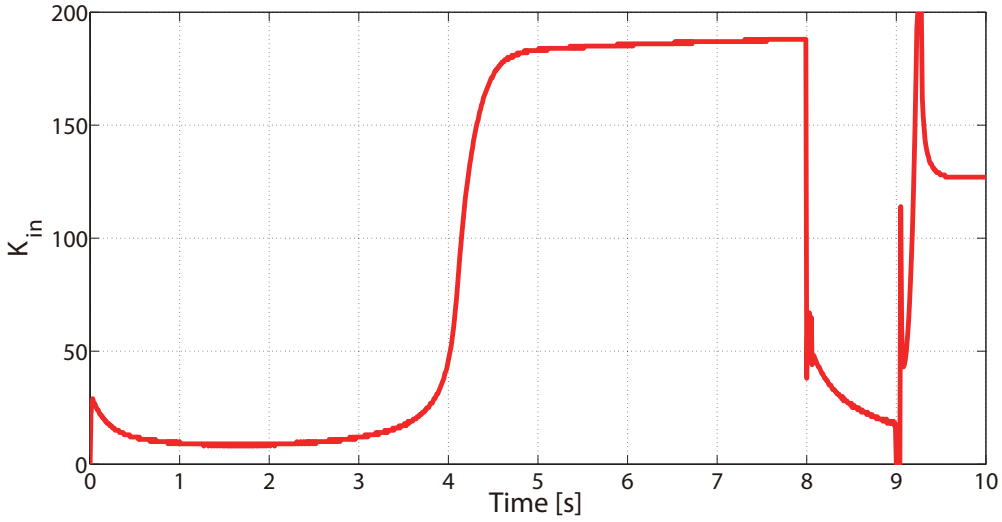

Figure 5.10 Time response of K_{in} for MP-SMC-I ($M = 1100$[kg])

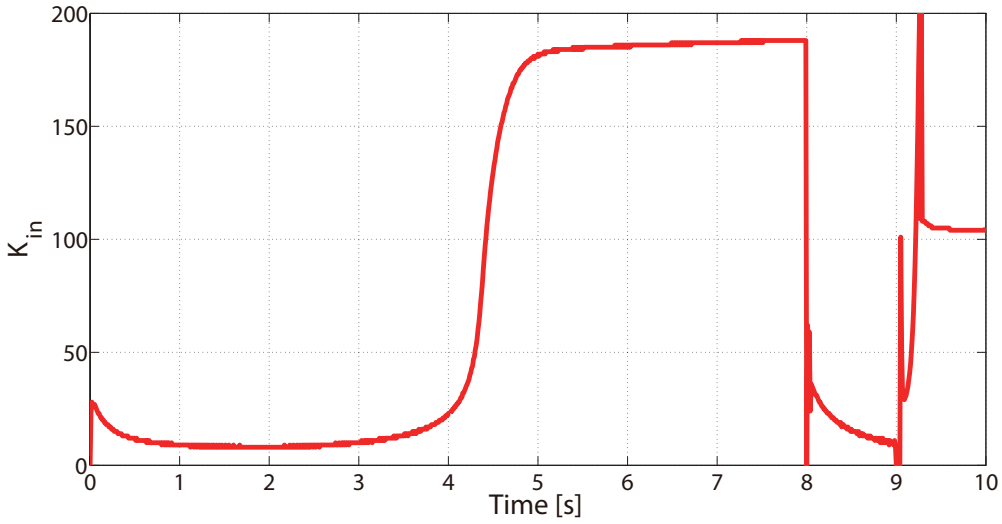

Figure 5.11 Time response of K_{in} for MP-SMC-I ($M = 1200$[kg])

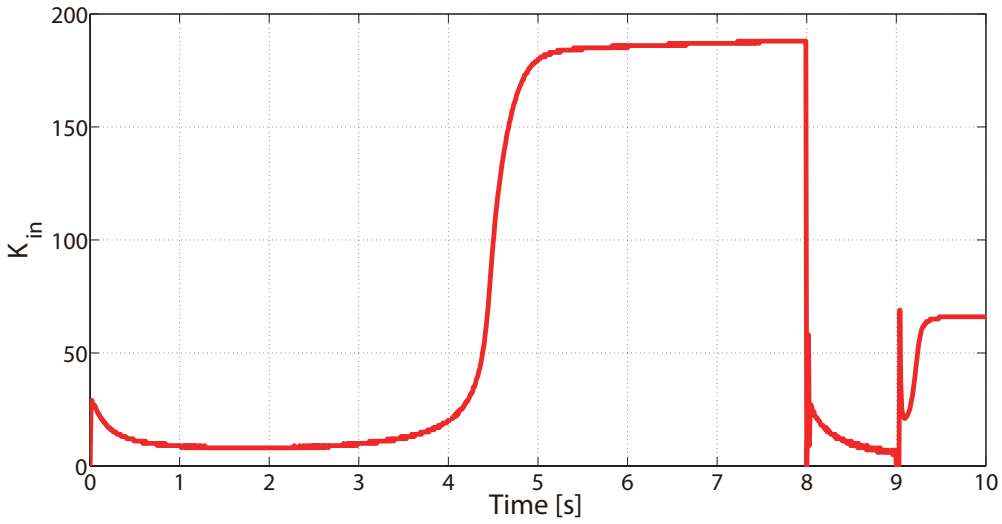

Figure 5.12 Time response of K_{in} for MP-SMC-I ($M = 1300$[kg])

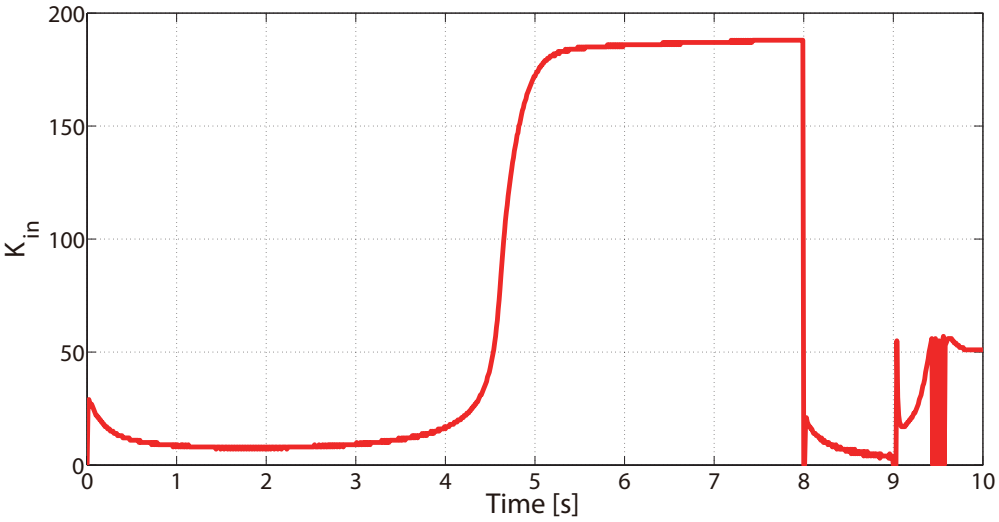

Figure 5.13 Time response of K_{in} for MP-SMC-I ($M = 1400$[kg])

Results of Acceleration Performance

To confirm the acceleration performance, we compare MP-SMC-I with SMC-I, SMC and No control. As shown in Figures 5.14∼5.18, the curve of the vehicle velocity with MP-SMC-I coincides with the one with SMC-I almost. But we can see that the vehicle with MP-SMC-I represented by the red curve achieves the maximum driving force for the best acceleration during the whole simulation time.

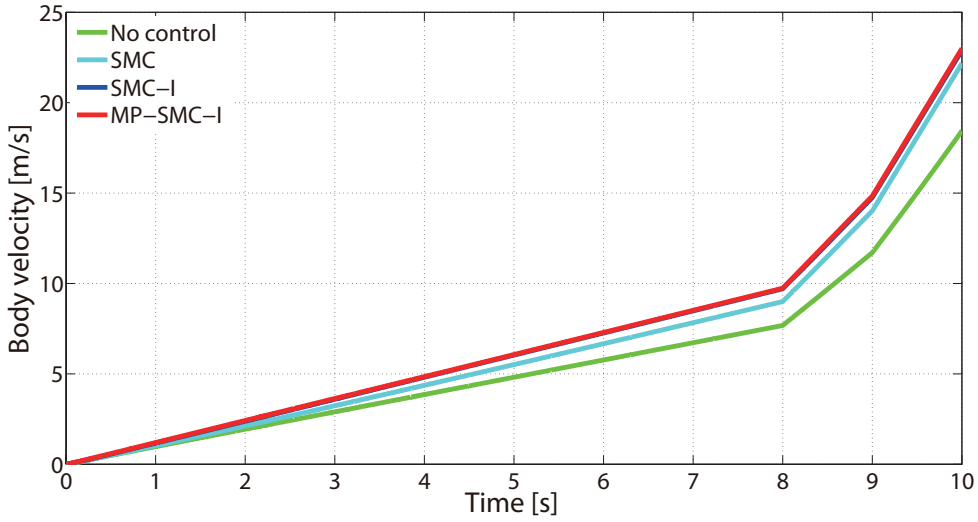

Figure 5.14 Time response of body velocity with No control, SMC, SMC-I and MP-SMC-I ($M = 1000$[kg])

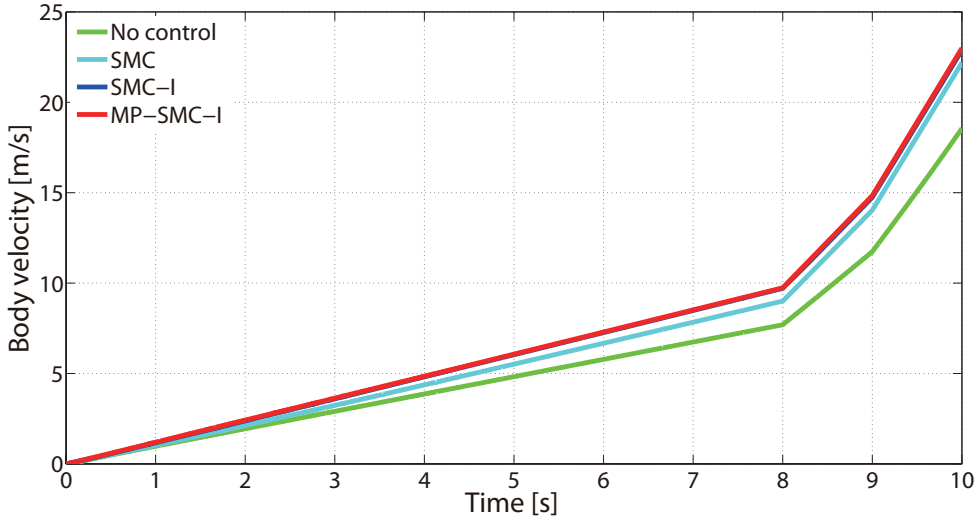

Figure 5.15 Time response of body velocity with No control, SMC, SMC-I and MP-SMC-I ($M = 1100$[kg])

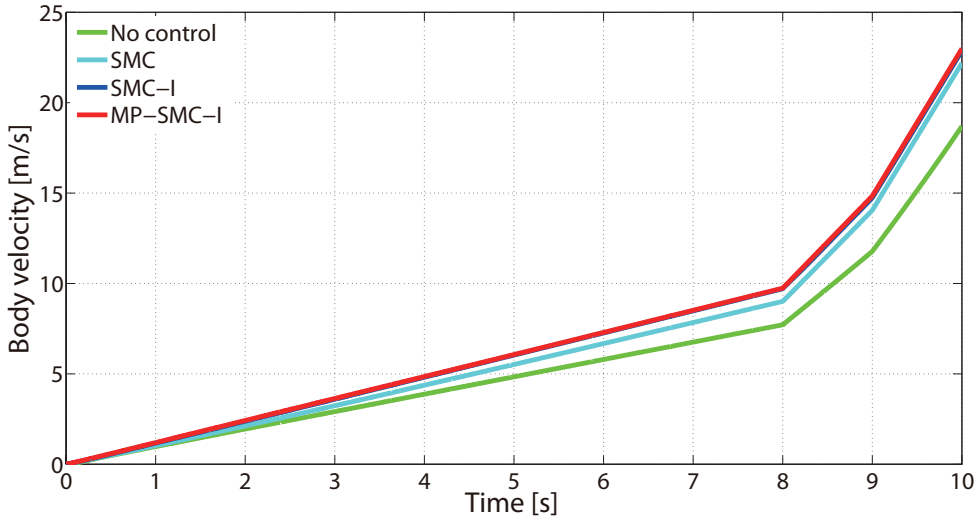

Figure 5.16 Time response of body velocity with No control, SMC, SMC-I and MP-SMC-I ($M = 1200$[kg])

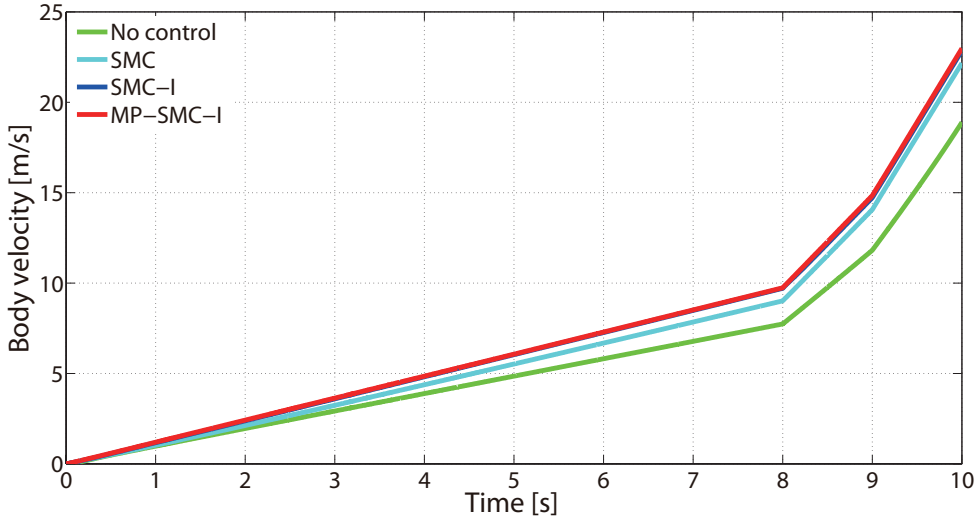

Figure 5.17 Time response of body velocity with No control, SMC, SMC-I and MP-SMC-I ($M = 1300$[kg])

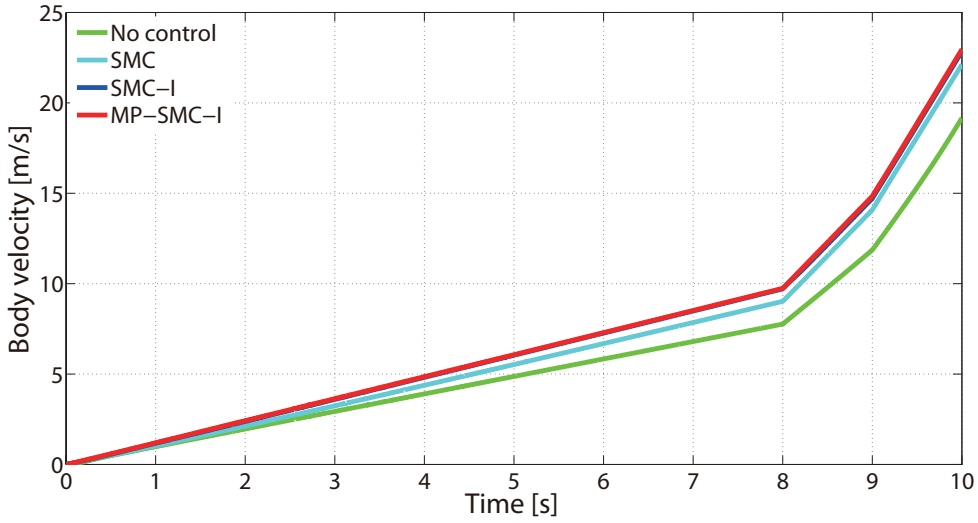

Figure 5.18 Time response of body velocity with No control, SMC, SMC-I and MP-SMC-I ($M = 1400$[kg])

Results of Energy Conservation Performance

In this section, to verify the effectiveness of MP-SMC-I, the simulation has been done during 10[s] as previous simulation setting, then the results are compared with SMC-I, SMC and No control. Tables 5.2∼5.5 show the results of the energy consumed E_r, the total distance D_d and the average energy consumption rate E_p for different mass of vehicle. The data of No control, SMC and SMC-I given here is just all the same thing as presented in chapter 4. We can see that the energy consumption rate with MP-SMC-I is nearly as much as the one with SMC-I, but the total distance is longer than SMC-I. This indicates that the vehicle with MP-SMC-I achieve a better acceleration performance. As the same result as the previous chapter described, due to the mass increasing caused much energy cost that the EV should be made

Table 5.2 Results of energy consumption rate with No control, SMC, SMC-I and MP-SMC-I ($M = 1000$[kg])

	E_r [Wh]	D_d [m]	E_p [Wh/km]
No control	80.34	55.52	1447
SMC	28.30	64.82	437
SMC-I	28.11	69.58	404
MP-SMC-I	28.64	70.03	409

Table 5.3 Results of energy consumption rate with No control, SMC, SMC-I and MP-SMC-I ($M = 1100$[kg])

	E_r [Wh]	D_d [m]	E_p [Wh/km]
No control	76.03	55.67	1366
SMC	30.13	64.87	464
SMC-I	30.15	69.58	433
MP-SMC-I	30.73	70.04	439

more light without detriment to performance.

Table 5.4 Results of energy consumption rate with No control, SMC, SMC-I and MP-SMC-I ($M = 1200$[kg])

	E_r [Wh]	D_d [m]	E_p [Wh/km]
No control	71.67	55.85	1283
SMC	31.89	64.92	491
SMC-I	32.18	69.57	463
MP-SMC-I	32.80	70.04	468

Table 5.5 Results of energy consumption rate with No control, SMC, SMC-I and MP-SMC-I ($M = 1300$[kg])

	E_r [Wh]	D_d [m]	E_p [Wh/km]
No control	67.25	56.07	1199
SMC	33.55	64.96	516
SMC-I	34.21	69.55	492
MP-SMC-I	34.86	70.03	498

Table 5.6 Results of energy consumption rate with No control, SMC, SMC-I and MP-SMC-I ($M = 1400$[kg])

	E_r [Wh]	D_d [m]	E_p [Wh/km]
No control	62.75	56.33	1114
SMC	35.10	64.98	540
SMC-I	36.22	69.54	521
MP-SMC-I	36.90	70.02	527

5.4 Summary

This chapter presents the MP-SMC-I method for slip suppression of EVs using slip ratio during the acceleration. This method focuses on determining the sliding surface parameter k_{in} adaptively based on MPC algorithm. The effectiveness of the method has been confirmed by numerical simulations.

The proposed method can suppress the slip ratio to the desired value on three different road conditions (dry asphalt road, wet asphalt road and icy road) with the mass distinct from the nominal mass to enhance acceleration performance by the nearly same energy consumption compared with SMC-I. That is, this method behaves a good robustness to different road conditions and load conditions. Especially, from the simulation results, we can say that the proposed method performs a profound effect on safety by suppressing the wheel slip when the vehicle is running on the slippery road conditions.

Chapter 6

Conclusion and Future Work

6.1 Conclusion

This dissertation has presented a robust control method for slip suppression of EVs during the acceleration from modeling to the development of simulation. This method focuses on improving the traveling performance and energy consumption performance by suppressing the slip ratio of wheel to a reference value, while the vehicle can achieve the maximum driving force on various road surfaces within a range of mass.

Chapter 2 described the general concept of SMC and discussed the robustness of SMC by implementation of an example.

Chapter 3 gave a description of the slip suppression control problem based on slip ratio, where the vehicle dynamics of one wheel model assumed as an in-wheel motor was presented. Then the reference value of slip ratio derived from the Magic-Formula was used in the slip ratio control.

In chapter 4, we proposed an extended SMC method by adding an integral item with gain K_{in} (SMC-I) to improve the acceleration performance and energy consumption performance of the slip suppression control by reducing the steady error of the slip ratio. SMC-I was conducted robustly on the control system with parameter uncertainties in the mass of the vehicle and road surface condition. The effectiveness of SMC-I was confirmed by numerical simulation. For SMC-I, K_{in} was a constant determined by trial and error. The problem we met was developing a systematic method to get the optimal value of K_{in}.

In chapter 5, SMC-I based on MPC algorithm was presented to determine the optimum K_{in}, which was adjusted on-line to improve the control performance further. The simulation were done and the results indicated the effectiveness of the method.

6.2 Directions for Future Work

In this dissertation, the constraints on the motor torque were not considered. In future work, we need to redefine the objective function under the torque constraint and to derive the new sliding control law. In addition, it is expected that MP-SMC-I method could be expanded for different driving modes (i.e., acceleration, cruise and deceleration). It is also intended to prepare and apply to more detailed vehicle model to promote the practicability.

At last, the basic framework of the proposed control method can be applied as it is and can also be expanded relatively easily to the foundation for making practical EVs with high performance and safety traction control systems and promoting further process. We expect it to play a role in promoting the widespread use of EVs.

Acknowledgments

I would like to express my gratitude to my adviser, Professor Tohru Kawabe, for providing an excellent environment for research and study, and for his guidance, encouragement and support. His rigorous scholarship to improve work style has deeply infected and inspired me, and this has led to my development as an engineer and a researcher.

I am also grateful to the excellent instruction and encouragement I have received from all of my professors at University of Tsukuba. Particularly, I would like to thank my dissertation committee and qualifying exam committee of Professor Takahito Kuno, Professor Akihisa Ohya, Professor Keisuke Kameyama and Professor Makoto Itoh for spending the time to review this dissertation and for their valuable suggestions helping me to pull together various concepts into a coherent picture to shape this document.

Thanks to all of members in Advanced Control System Research Group (ACSRG) for the advice, companionship and conversation over the past six years. In particular, many thanks to Ph.D Ko Nakamura for his detailed comments, suggestions about the research and for making the lab a very unique place to work and just debate ideas.

I would like to especially thank my parents and my sister for their constant support and encouragement.

References

[1] D. Wilson, R. Purushothaman and T. Fiotakis, The BRICs and Global Markets: Crude, Cars and Capital, Goldman Sachs, USA, 2004.

[2] J. Dargay, D. Gately and M. Sommer, “Vehicle Ownership and Income Growth, World-wide: 1960-2030”, The Energy Journal, vol. 28, no. 4, pp. 143-170, 2007.

[3] W. Beckerman, “Economic Growth and the Environment: Whose Growth? Whose Environment?”, World Development, vol. 20, no. 4, pp. 481-496, 1992.

[4] A. G. Mamalis, K. N. Spentzas and A. A. Mamali, “The Impact of Automotive Industry and Its Supply Chain to Climate Change: Somme Techno-economic Aspects”, European Transport Research Review, vol. 5, no. 1, pp. 1-10, 2013.

[5] S. Brown, D. Pyke and P. Steenhof, “Electric Vehicles: the Role and Importance of Standards in an Emerging Market”, Energy Policy, vol. 38, no. 7, pp. 3797-3806, 2010.

[6] T. Hirota, M. Ueda and T. Futami, “Activities of Electric Vehicles and Prospect for Future Mobility”, Journal of SICE, vol. 50, no. 3, pp. 165-170, 2011 (in Japanese).

[7] H. Tseng, J. S. Wu and X. Liu, “Affordability of Electric Vehicle for a Sustainable Transport System: An Economic and Environmental Analysis”, Energy Policy, vol. 61, pp. 441-447, 2013.

[8] The official U.S. government source for fuel economy information, All Electric Vehicles (EVs), “http://www.fueleconomy.gov/feg/evtech.shtml”, January 3, 2015.

[9] The official Teslamotors website for Model S, “http://www.teslamotors.com/models”, January 3, 2015.

[10] S. Sakai, Y. Hori, “Advanced Vehicle Motion Control of Electric Vehicle Based on the Fast Motor Torque Response”, Proceedings of the 5th Annual International Symposium on Advanced Vehicle Control, pp. 729-736, 2000.

[11] K. Miyake, I. Yamaki and T. Fujita, “Four Wheel Anti-Lock Brake System (ABS) for Four-Wheel Drive Vehicles”, SAE Technical Paper, Paper No. 880322, 1988.

[12] T. Tanaka, K. Isoda and M. Ohsaki, “Traction Control System for Improved Driving Safety”, SAE Technical Paper, Paper No. 912583, 1991.

[13] A. T. Zanten, R. Erhardt and G. Pfaff, “VDC, The Vehicle Dynamics Control System of Bosch”, SAE Technical Paper, Paper No. 950759, 1995.

[14] S. Inagaki, “Improvement for Active Safety Performance of Toyota VSC”, Jounal of JSME, vol. 106, no. 1012, pp. 154-155, 2003 (in japanese).

[15] K. Kin, T. Ikeda and O. Yano, “Improvements in Handling on a Slippery Road with VSA”, Honda R&D Technical Review, vol. 13, no. 2, pp. 83-90, 2001 (in Japanese).

[16] K. Sawase, Y. Ushoroda and T. Miura, “Left-Right Torque Vectoring Technology as the Core of Super All Wheel Control (S-AWC)”, Mitsubishi Motors Technical Review, no. 18, pp. 18-24, 2006 (in Japanese).

[17] M. Shino, M. Nagai, “Independent Wheel Torque Control of Small-Scale Electric Vehicle for Handing and Stability Improvement”, JSAE Review, vol. 24, no. 4, pp. 449-456,

2003.

[18] L. Yuan, H. Chen and B. Ren, “The Design of TCS Controller for Four Wheel Independent-Drive Electric Vehicle Based on ADRC”, Proceedings of the 26th Chinese Control and Decision Conference (CCDC 2014), pp. 2638-2643, 2014.

[19] S. Kodama, L. Li and Y. Hori, “Skid Prevention for EVs Based on the Emulation of Torque Characteristics of Separately-wound DC Motor”, Proceedings of the 8th IEEE International Workshop on Advanced Motion Control, pp. 75-80, 2004.

[20] M. Mubin, S. Ouchi, M. Anabuki and H. Hirata, “Drive Control of an Electric Vehicle by a Non-linear Controller”, IEEJ Transactions on Industry Applications, vol. 126, no. 3, pp. 300-308, 2006 (in Japanese).

[21] K. Fujii and H. Fujimoto, “Slip Ratio Control Based on Wheel Control without Detection of Vehicle Speed for Electric Vehicle”, IEEJ Technical Meeting Record, pp. 27-32, 2007 (in Japanese).

[22] Y. Hori, “Simulation of MFC-Based Adhesion Control of 4WD Electric Vehicle”, IEEJ Record of Industrial Measurement and Control, vol. IIC-00, no. 1-23, pp. 67-72, 2000 (in Japanese).

[23] T. Kawabe, Y. Kogure, K. Nakamura, K. Morikawa and T. Arikawa, “Traction Control of Electric Vehicle by Model Predictive PID Controller”, Transaction of JSME Series C, vol. 77, no. 781, pp. 3375-3385, 2011 (in Japanese).

[24] V. Utkin, “Variable Structure Systems with Sliding Modes”, IEEE Transactions on Automatic Control, vol. 22, no. 2, pp. 212-222, 1977.

[25] H. Tan, Y. Chin, “Vehicle Traction Control: Variable Structure Control Approach”, Jour-

nal of Dynamic Systems, Measurement and Control, vol. 113, no. 2, pp. 223-230, 1991.

[26] M. Amodeo, A. Ferrara, R. Terzaghi and C. Vecchio, “Wheel Slip Control Via Second-order Sliding-mode Generation”, IEEE Transactions on Intelligent Transportation Systems, vol. 11, no. 1, pp. 122-131, 2010.

[27] C. Ünsal, “Sliding Mode Measurement Feedback Control for Antilock Braking Systems”, IEEE Transactions on Control Systems Technology, vol. 7, no. 2, pp. 271-281, 1999.

[28] J. E. Slotine, W. Li, Applied Nonlinear Control, Prentice Hall, USA, 1991.

[29] S. Li, T. Kawabe, “Slip Suppression of Electric Vehicles Using Sliding Mode Control Method”, Journal of Intelligent Control and Automation, vol. 4, no. 3, pp. 327-334, 2013.

[30] J. Richalet, A. Rault, J. L. Testud and J. Papon“Algorithmic Control of Industrial Processes”, Proceedings of the 4th IFAC Symposium on Identification and System Parameter Estimation, pp. 1119-1167, 1976.

[31] J. Richalet, A. Rault, J. L. Testud and J. Papon“Model Predictive Heuristic Control: Application to Industrial Processes”, Automatica, vol. 14, no. 5, pp. 413-428, 1978.

[32] D. W. Clarke, “Application of Generalized Predictive Control to Industrial Processes”, IEEE Control Systems Magazine, vol. 8, no. 2, pp. 49-55, 1988.

[33] C. E. García, D. M. Prett and M. Morari, “Model Predictive Control: Theory and Practice - A Survey”, Automatica, vol. 25, no. 3, pp. 335-348, 1989.

[34] E. Zafiriou, “Robust Model Predictive Control of Processes with Hard Constraints”, Comupter and Chemical Engineering, vol. 14, no. 4-5, pp. 359-371, 1990.

[35] J. Gómez Ortega, E. F. Camacho, “Mobile Robot Navigation in a Partially Structured Static Environment Using Neural Predictive Control”, Control Engineering Practice, vol. 4, no. 12, pp. 1669-1679, 1996.

[36] W. Gabin, D. Zambrano and E. F. Camacho, “Sliding Mode Predictive Control of a Solar Air Conditioning Plant”, Control Engineering Practice, vol. 17, no. 6, pp. 652-663, 2009.

[37] S. Gao, L. Luan, “The PVC Stripping Process Predictive Control Based on the Implicit Algorithm”, Mathematical Problems in Engineering, vol. 2014, Artical ID 838404, 8 pages, 2014.

[38] V. V. Naik, D. N. Sonawane, D. D. Ingole and D. Ginoya, “Model Predictive Control of DC Servomotor Using Active Set Method”, Proceedings of 2013 IEEE International Conference on Control Applications (CCA 2013), pp. 820-825, 2013.

[39] Y. Cong, “Model Predictive Control for Vehicle Emergency Motion Planning Based on Flatness”, Proceedings of the 30th Chinese Control Conference (CCC 2011), pp. 3543-3548, 2011.

[40] V. Utkin, Sliding Modes and Their Applications in Variable Structure Systems, Mir Publishers, USSR, 1978.

[41] U. M. Ch, Y. S. K. Babu and K. Amaresh, “Sliding Mode Speed Control of a DC Motor”, Proceedings of 2011 International Conference on Communication Systems and Network Technologies (CSNT 2011), pp. 387-391, 2011.

[42] K. Nakano, U. Sawut, K. Higuchi and Y. Okajima, “Modelling and Observer-based Sliding-mode Control of Electronic Throttle Systems”, Transaction on Electrical Engi-

neering, Electronics and Communications, vol. 4, no. 1, pp. 22-28, 2006.

[43] Y. Li, J. O. Lee and J. Lee, “Attitude Control of the Unicycle Robot Using Fuzzy-sliding Mode Control”, Proceedings of the 5th International Conference on Intelligent Robotics and Applications (ICIRA 2012), vol. 3, pp. 62-72, 2012.

[44] H. B. Pecejka, E. Bakker, “The Magic Formula Tyre Model”, Proceedings of the 1st International Colloquium on Tyre Models for Vehicle Dynamics Analysis, pp. 1-18, 1991.

[45] E. F. Camacho, C. B. Alba, Model Predictive Control (2nd ed.), Springer-Verlag, USA, 2003.

[46] J. M. Maciejowski, S. Adachi and M. Kanno (Eds.), Predictive Control with Constraints, Tokyo Denki University Press, Japan, 2005 (in Japanese).

List of Publications

Research Achievement

Journal Articles

1. Shaobo Li and Tohru Kawabe, “Slip Suppression of Electric Vehicles Using Sliding Mode Control Based on MPC Algorithm”, International Journal of Engineering and Industries, vol. 5, no. 4, pp. 11-23, 2014.
2. Shaobo Li and Tohru Kawabe, “Slip Suppression of Electric Vehicles Using Sliding Mode Control Method”, International Journal of Intelligent Control and Automation, vol. 4, no. 3, pp. 327-334, 2013.

Refereed Conference Papers

1. Shaobo Li, Ko Nakamura and Tohru Kawabe, “A Sliding Mode Control Based on MPC Algorithm for Slip Ratio of Electric Vehicle”, Proceedings of the SICE Annual Conference 2014 (SICE 2014), pp. 710-714, Sapporo, Japan, September, 2014.

2. Shaobo Li and Tohru Kawabe, “Sliding Mode Slip Suppression Control of Electric Vehicles”, Proceedings of the 10th International Conference on Informatics in Control, Automation and Robotics (ICINCO 2013), vol. 2, pp. 11-18, Reykjavik, Iceland, July, 2013.
3. Shaobo Li, Ko Nakamura, Tohru Kawabe and Koichi Morikawa, “A Sliding Mode Control for Slip Ratio of Electric Vehicle”, Proceedings of the SICE Annual Conference 2012 (SICE 2012), pp. 1974-1979, Akita, Japan, August, 2012.